Journal of
Cardiovascular Development and Disease

MDPI

Article

Cardiac Neural Crest and Endocardial-to-Mesenchymal Transition Dysfunction Links Bicuspid Aortic Valve Formation to Adult Aortopathy

María Teresa Soto-Navarrete [1,2,*,†], Bárbara Pozo-Vilumbrales [3,4,†], Ana Carmen Durán [3,4] and Borja Fernández [2,3,4]

[1] Intercellular Signalling in Cardiovascular Development & Disease Laboratory, Centro Nacional de Investigaciones Cardiovasculares Carlos III (CNIC), 28029 Madrid, Spain
[2] CIBER de Enfermedades Cardiovasculares (CIBERCV), 28029 Madrid, Spain; borjafe@uma.es
[3] Department of Animal Biology, Faculty of Science, University of Málaga, 29071 Málaga, Spain; barbarapovi@uma.es (B.P.-V.); acduran@uma.es (A.C.D.)
[4] Biomedical Research Institute of Málaga and Platform on Nanomedicine (IBIMA-Plataforma BIONAND), 29590 Málaga, Spain
* Correspondence: mtsoto@cnic.es
† These authors contributed equally to this work.

Abstract

The aortic wall of patients with aortic dilatation (AD) associated with a bicuspid aortic valve (BAV) shows signs of embryonic endothelial-to-mesenchymal transition (EndMT), suggesting that EndMT initiates bicuspid aortopathy. EndMT underlies embryonic valvulogenesis, so it might be the link between BAV and AD, but a mechanistic explanation is missing. In a recent proteomic analysis (PMID: 39832690), we found molecular alterations in the ascending aorta of the BAV hamster model, similar to those described in patients. However, we did not find evidence of EndMT. Hamster embryonic studies have shown that BAV emerges from disrupted EndMT during cardiac outflow tract (OFT) septation, likely triggered by aberrant cardiac neural crest (CNC) cells (PMID: 40074779), but the EndMT-specific molecular signaling was not addressed. We aimed here (1) to reanalyze the original hamster proteomic dataset to search for EndMT, and (2) to assess EndMT and its signaling regulation during murine OFT septation. The results showed (1) specific EndMT and CNC cell molecular alterations in the aorta of affected hamsters associated with genetics and hemodynamics, and (2) NOTCH1-dependent regulation of EndMT during murine septation. We propose that BAV aortopathy etiology relies on genetic defects that affect CNC cell induction of EndMT, leading to BAV in the embryo, and aortic CNC-derived SMC differentiation, predisposing to adult AD. Defective CNC-derived SMCs may reactivate embryonic EndMT in the adult aorta, exacerbated by hemodynamics in individuals with BAV.

Keywords: bicuspid aortic valve; aortopathy; endothelial-mesenchymal transition; fetal gene hypothesis; cardiac neural crest; hamster model

Check for updates

Academic Editors: Jörg Männer and Robert H. Anderson

Received: 15 September 2026
Revised: 8 November 2026
Accepted: 10 November 2026
Published: 14 November 2026

Copyright: © 2026 by the authors. Licensee MDPI, Basel, Switzerland. This article is an open access article distributed under the terms and conditions of the Creative Commons Attribution (CC BY) license.

1. Introduction

Graphical Abstract. Mechanistic model of bicuspid aortic valve (BAV) aortopathy in the hamster. The ascending aorta and aortic valve formation occurs during septation of the embryonic cardiac outflow tract (OFT). Three cell lineages participate in this process: second heart field (SHF; in red), cardiac neural crest (CNC; in green) and endocardial (in blue)

derived cells. In the outbred H control strain, with tricuspid aortic valve (HTAV), normal CNC cells are responsible for inducing the fusion of conal ridges (CRs), which occurs by endocardial-mesenchymal transition (EndMT), leading to the septation of the OFT and the formation of a TAV. SHF and CNC cells will differentiate in smooth muscle cells (SMC) of the adult aorta. We hypothesize that the inbred T strain, with 40% of BAV and 100% aortic dilatation (AD) carries a genetic defect that affects the CNC cells migration during OFT septation, and the aortic CNC-derived SMC differentiation. In TBAV animals, this defect extends the area of endocardial cells that underly EndMT during the fusion of CRs, leading to BAV and altered CNC-derived SMCs in the adult ascending aorta, predisposing to structural alterations (SMC phenotypic switch and apoptosis). In TTAV hamsters, the genetic defect does not affect the valve morphology likely due to epigenetic and embryonic stochastic factors, but it does alter CNC-derived SMCs. We propose that these altered CNC-derived SMC may reactivate the embryonic EndMT process in the endocardium of the adult ascending aorta (and possibly the apoptosis of CNC-derived SMCs), being exacerbated by hemodynamics in those individuals carrying a BAV.

Bicuspid aortic valve (BAV) is the most prevalent human congenital cardiac malformation, with an incidence of 1–2% in the general population. BAV is an inherited condition that can be asymptomatic, but most carriers develop valvulopathies and aortopathies for which no pharmacological therapies exist. Surgical intervention is the only effective treatment. As recognized by specialists, the lack of medical therapy besides surgery relies on a limited understanding of the pathological mechanisms and factors triggering the onset of the disease [1,2].

The histopathology of BAV aortopathy is defined as medial necrosis, i.e., elastic fiber fragmentation; smooth muscle cell (SMC) apoptosis; and accumulation of mucoid material in acellular spaces [2,3]. This condition leads to progressive aortic dilatation (AD), which entails a high risk of arterial wall rupture and sudden death due to 'inherent weakness in the arterial wall' [2,3]. This assertion reflects the widely accepted hypothesis that the etiology of bicuspid aortopathy has two clear components, genetics and hemodynamics. The current consensus is that anomalies of the hemodynamic pattern in the ascending aorta, caused by the disturbed flow created by the abnormal valve morphology, impact the congenitally defective arterial wall, altering the vascular matrix homeostasis and inducing vessel remodeling [4–8]. Although we know much about the hemodynamic alterations and the histopathological changes taking place in the dilating ascending aorta, the causes and nature of the inherent aortic wall abnormality remain unclear.

It is believed that aortic wall defects in BAV patients lie in the embryology of the cardiac outflow tract (OFT), where the cardiac neural crest (CNC) plays key roles in the development of both the valve and the ascending aorta. Indeed, many valve interstitial cells and aortic SMCs derive from this embryonic cell population [9–11]. Therefore, currently the term "BAV syndrome" is considered more appropriate to describe a disease caused by structural alterations of the valve and the aorta induced by defective behaving CNC cells [1,12,13].

In recent years, a plethora of evidence has emerged pointing to epithelial-mesenchymal transition (EMT) as the initiator of ascending aorta degeneration in BAV patients [14,15]. EMT is a fundamental, evolutionarily conserved mechanism involved in the morphogenesis of metazoans. It is basically an embryonic process, but it can be reactivated in adult tissues during repair and disease. When occurring in endocardial or endothelial cells, this process is referred to as EndMT. Research on EMT and EndMT has significantly increased in the last decade due to the discovery of their involvement first in cancer pathogenesis and tissue fibrosis [16], and later in different cardiovascular pathologies, including atherosclerosis and possibly bicuspid aortopathy [17,18].

In 2023, a GWAS study in patients found a risk locus for human BAV in the *Mucin4* gene [19], which encodes a protein involved in EMT, but no functional validation has been obtained in mutant mice to date. Studies of aortic samples from BAV patients have shown increased expression of EMT genes and additional molecular signatures of EndMT, including activation of ZEB1, NOTCH1 and RHOA, as well as alterations in VE-cadherin expression [14,15,20]. Enrichment analysis of patient proteomic datasets confirmed these results, highlighting alterations in the adult defective aorta of pathways associated specifically with embryonic EndMT and, interestingly, with CNC embryonic cell migration [21,22]. A study of the ultrastructure of the dilated aorta of patients with BAV revealed endothelial cell junction fragility, complex pseudopodia formation, and abundant stress fibers [22]. All these data provide evidence for a process compatible with the initial phase of EndMT in the ascending aorta of BAV patients [22,23]. The collective outcome of changes associated with EndMT in the aortic wall would result in mural cells with mesenchymal characteristics and inherent instability in the aorta, contributing to the development of aortopathy [22]. Consequently, the notion of EndMT as an embryological cellular mechanism reactivated in the adult ascending aorta of patients with BAV has been proposed [14,21–23]. Given the established role of EndMT in the development of the aortic valve primordia, it is conceivable that this cellular process serves as a link between the embryonic valve defect and adult AD. However, a mechanistic explanation for this association remains elusive.

In a recent study using the well-established BAV hamster model, we have shown that the embryonic defect responsible for antero-posterior (AP) BAV formation involves an alteration in the EndMT normally occurring in the embryonic cardiac OFT, caused by defective behavior of CNC cells [24,25]. However, the conclusions of that study rely mainly on morphological evidence of the cellular mechanisms involved in EndMT at the OFT. The EndMT-specific molecular signaling was not addressed, due to the lack of experimental tools suitable for the hamster model.

Together with BAV, animals in this model present with non-aneurysmal dilation of the ascending aorta, exhibiting histopathological and molecular alterations analogous to those observed in human AD [26]. In a recent comparative proteomic study of the hamster ascending aorta, changes in the protein content associated with hemodynamic and genetic factors were characterized independently [27]. While the former reflected many of the molecular alterations identified in affected patients, indicating a central role for the PI3K-AKT pathway, enrichment analysis of the proteomic data revealed that the Wnt/β-catenin molecular pathway, which is one of the main intracellular regulators of EndMT, was the most significantly altered in the aortas of genetically predisposed animals.

In the present study, we have reanalyzed our previous proteomic data in search of evidence that EndMT is affected in the ascending aorta of the BAV hamster model. In addition, we show new evidence on the signaling regulation of EndMT in the embryonic valve primordia of the mouse. We discuss these new pieces of evidence, the combination of which allows us to propose a model of BAV disease based on the so-called 'fetal gene hypothesis'.

2. Material and Methods

2.1. Quantitative Proteomics

The present proteomic study was based on a secondary analysis of a previously published proteomic dataset, which had been generated from ascending aortic tissue of Syrian hamsters (*Mesocricetus auratus*) belonging to the T strain, with 40% spontaneous AP BAV and fully penetrant AD, and a control outbred strain (H) with 100% normal or tricuspid aortic valve (TAV) and normal ascending aorta [24–32]. The experimental procedures for sample collection, protein extraction, mass spectrometry acquisition, and primary data processing have been previously described in detail [27].

The proteomic study comprises 18 ascending aortic samples obtained from individuals aged approximately 300 days, which were distributed across three experimental groups: animals from the T strain with BAV (TBAV, n = 6) and with TAV (TTAV, n = 6); and animals from the control strain with TAV (HTAV, n = 6). Protein concentration was determined using a Qubit 4 Fluorometer (Thermo Fisher Scientific, Massachusetts, MA, USA), and 50 µg of protein from each biological replicate was subjected to proteomic analysis. Subsequent to the process of enzymatic digestion, the peptides were analyzed using an Easy nLC 1200 ultra-high-performance liquid chromatography (UHPLC) system, which was coupled to a Q Exactive HF-X Orbitrap mass spectrometer (Thermo Fisher Scientific, USA). The acquisition of data was conducted over an m/z range of 375–1600 at a resolution of 120,000. Peptide identification was conducted against the *M. auratus* NCBI protein database, and protein quantification was performed using a label-free approach.

2.2. Bioinformatic Analysis

The raw proteomic dataset generated in the original study was subjected to reanalysis using a modified protein inclusion strategy. In contrast to the original analysis [27], which considered only proteins detected in all three biological replicates within each comparison, the present study included proteins detected in a minimum of two of the three biological replicates in each experimental group. The adoption of this less restrictive filtering criterion was driven by the objective of enhancing proteome coverage while preserving reproducibility across biological replicates.

The analysis of differential protein expression was conducted by means of $\log_2$-transformed standardized protein abundances. The thresholds employed to define differentially expressed proteins were consistent with those implemented in the original study, requiring an absolute log2 fold change ≥ 1 and a false discovery rate (FDR)-adjusted p-value < 0.05. Functional enrichment was carried out using the STRING database, Gene Ontology enrichment, Enrichr database, and Ingenuity Pathway Analysis (IPA), as previously described [27].

2.3. Embryo Processing

C57BL/6 mouse embryos were harvested at E11.5 (n = 10) and E12.5 (n = 3), euthanized in ice-cold phosphate-buffered saline, and fixed in 4% paraformaldehyde overnight at 4 °C. For paraffin embedding, embryos were dehydrated through a graded ethanol series, xylene washes, and a xylene-paraffin step, and embedded in paraffin to obtain transverse and frontal sections of the heart. Animals were handled according to European guidelines (Directive 2010/63/EU) and Spanish regulations (R.D. 53/2013; B.O.E. 01.02.2013).

2.4. Histochemistry and Immunofluorescence

Sections (7 µm) were deparaffinized and hydrated in a graded ethanol series. For basic histological analysis, E11.5 and E12.5 embryos were stained with hematoxylin-eosin or Alcian blue-fast red following standard protocols. Bright-field images were obtained with an Olympus BX51 microscope or a Leica DMSL microscope. For immunofluorescence, sections from E11.5 embryos were boiled in citrate buffer pH 6 for antigen retrieval for 15 min, blocked for endogenous peroxidases with 3% H_2O_2 for 30 min, and blocked for nonspecific binding with 10% fetal bovine serum for 1h. Hereafter, primary antibodies (anti-N1ICD, anti-ERG 647, and anti-SMA Cy3; Table S1) were incubated overnight at 4 °C, followed by 1-h incubation with anti-rabbit biotinylated secondary antibody at RT. Then, samples were incubated with AB complex (Vector Labs, Newark, CA, USA) for 30 min and stained with tyramide signal amplification (TSA) (Thermo Fisher Scientific, USA).

Nuclei were stained with DAPI. Coverslips were mounted with Fluoromount (Thermo Fisher Scientific, USA), and images were obtained on a Leica SP8 confocal microscope.

3. Results

3.1. Proteomic Reanalysis in Hamster Adult Aortas

3.1.1. TBAV vs. HTAV

We identified 2102 proteins in the aortas of TBAV and HTAV animals. Of these, 236 were found to be deregulated in the aortic tissue of BAV animals (100 with increased expression and 136 with decreased expression) (Figure 1A,B and Table S2). This set of proteins shows a significant protein-protein interaction (PPI) enrichment according to the STRING database (p-value = $4.75 \cdot 10^{-11}$), indicating that they interact more than expected for a random set of proteins (Figure 1C).

The analysis of differentially expressed proteins using the IPA software (Qiagen, Inc., 2024) revealed 174 enriched canonical pathways ($\log_{10}(p\text{-value}) > 1$) (Table S3). We conducted a general classification of these pathways into ten categories: Cytoskeleton organization, adhesion, and mechanotransduction; Growth factor, MAPK, and receptor tyrosine kinase signaling; Contractility-related signaling; Endothelial function, nitric oxide, and vascular signaling; Immune, inflammatory, and extracellular matrix remodeling; Cell stress, proteostasis, and cell death; Metabolism and bioenergetics; RNA/protein synthesis and gene regulation; Trafficking, endocytosis, and membrane dynamics; and Developmental and cell fate pathways. Interestingly, the term 'Regulation of the Epithelial-Mesenchymal Transition Pathway' emerged as significantly enriched ($-\log_{10}(p\text{-value}) = 1.59$) in the last category, with 14 proteins involved (TJP1, MAP2K4, VTN, MAP2K2, COL4A1, CTNNB1, KRAS, ROCK1, RHEB, EFEMP2, SGCD, SGCB, SLIT3, FBLN5). In a broader search, we detected 19 canonical pathways that were directly related to the EndMT process, including the PI3K-AKT pathway (Figure 1D). The IPA causal network analysis revealed dysregulation of key EMT regulatory proteins such as ZEB, ZEB2, SNAI1 and TWIST (p-values of 1.33×10^{-8}, 7.08×10^{-7}, 1.16×10^{-5}, and 1.13×10^{-4}, respectively) (Table 1).

Table 1. Proteins related to EndMT detected in IPA causal network analysis in each comparison.

	Master Regulator	Molecule Type	Participating Regulators	z-Score	p-Value of Overlap	Target Molecules in Dataset
TBAV vs. HTAV	ZEB	group	Akt, AKT1, ERK1/2, Jnk, MYC, Nfat (family), P38 MAPK, RB1, TP53, ZEB, ZEB1, ZEB2	0.801	1.33×10^{-8}	ACTB, ACTC1, AIP, AK1, CD55, CMA1, CYFIP2, DBT, DNAJA2, ECH1, EFEMP1, FBLN5, GC, GLS, HSPA5, IPO7, KRAS, LGMN, MACROH2A1, MAP2K2, NDUFS2, NOS3, NTN1, PAWR, PRPSAP1, PSMB6, PSMD8, RANBP1, RBBP7, ROCK1, RPL17, RPL18A, RPN1, SOD1, SPARCL1, STT3A, TJP1, TMED10, UBE2D1
	ZEB2	transcription regulator	Akt, AKT1, ERK1/2, Jnk, Nfat (family), P38 MAPK, RB1, ZEB2	0.655	7.08×10^{-7}	ACTB, ACTC1, AIP, C1QC, CD55, CMA1, COL4A1, CTNNB1, EGFR, HSPA5, LAMB2, MAP2K2, NDUFS2, NEXN, NOS3, PSMB6, SOD1, SPARCL1, STT3A, TJP1, TMED10
	SNAI1	transcription regulator	Akt, CDH1, MUC1, SNAI1, SP1, TAFAZZIN, YAP1	0.471	1.16×10^{-5}	ACADSB, ACTB, AEBP1, CD55, COX4I2, GSR, HSPA5, LAMB2, MECP2, PSMD8, RANBP1, SOD1, SPARCL1, STT3A, TJP1, TMED10, UBE2D3, USP5
	TWIST2	transcription regulator	TWIST2	0.000	1.13×10^{-4}	CTNNB1, FBLN5, HSPA5, PRKAA1

Table 1. *Cont.*

	Master Regulator	Molecule Type	Participating Regulators	z-Score	*p*-Value of Overlap	Target Molecules in Dataset
TTAV vs. HTAV	SOX2-OCT4-NANOG	complex	GLI1, NANOG, POU5F1, SNAI2, SOX2, SOX2-OCT4-NANOG, TP53	−0.832	3.40×10^{-5}	ADK, APOBEC2, CCDC80, CTNNB1, FERMT2, G3BP2, IPO7, MACROH2A1, NSFL1C, PTK2B, SERPINB9, TNC, UBE2D3
	LATS2	kinase	LATS2, SNAI1, TAFAZZIN, TP53, YAP1	−0.905	5.05×10^{-5}	APOBEC2, CCDC80, CTNNB1, FERMT2, IPO7, MACROH2A1, PTK2B, SERPINB9, SPARCL1, TNC, UBE2D3
	SOX2	transcription regulator	SOX2, TP53	−0.905	8.79×10^{-5}	APOBEC2, CCDC80, CTNNB1, EFEMP1, FERMT2, IPO7, MACROH2A1, NSFL1C, PTK2B, SERPINB9, TNC
	ZEB	group	Akt, ERK1/2, MYC, Nfat (family), TP53, ZEB, ZEB1, ZEB2	0.277	1.15×10^{-4}	APOBEC2, CCDC80, CMA1, EFEMP1, FERMT2, IPO7, KRAS, MACROH2A1, NT5E, PTK2B, PYCR1, SERPINB9, SPARCL1
	SOX1	transcription regulator	SOX1	1.414	5.08×10^{-3}	CTNNB1, EFEMP1
TBAV vs. TTAV	ZEB1	transcription regulator	BAX, BBC3, BCL2L1, CCND1, CDKN1B, CDKN2A, CHEK1, CREB1, EGFR, EIF2AK3, ERBB2, ERN1, FAS, FOXP3, HMGB2, HNF4A, IL6, INSR, KAT5, LAMC2, mir-19, MMP14, MTOR, MYC, NANOG, NRF1, PPIF, RUNX3, SERPINE1, SET, Tgf beta, TGFB1, TP53, UHRF1, USP7, XBP1, YAP1, ZEB1	1.753	1.33×10^{-9}	ACADSB, ACTB, ADD1, AIFM1, AK1, AMT, APCS, C1QC, CAT, CCDC80, CNP, COL4A1, Dazap1, DBT, DCTN4, DNAJA2, DNPEP, ECH1, EHD3, EIF6, FBLN5, FHL1, FILIP1L, FZD2, GLS, GOLGA3, GSK3B, LGMN, MACROH2A1, MAPK9, MTCH2, NEXN, NOS3, PPM1F, PRKAA1, PSMD6, PSMD8, PYCR1, RANBP1, RHEB, ROCK1, RPL17, RPN1, RPS2, SEC22B, SFN, SGCD, SHMT2, TM7SF2, TMED2, TNC, UBE2D1, UGDH, UGP2, WDR82
	TWIST	group	CDH1, TP53, TWIST, TWIST2	−0.784	1.23×10^{-7}	ACTB, AK1, ALB, C1QC, CCDC80, COL4A1, DBT, DNAJA2, ECH1, FBLN5, FHL1, GSK3B, GSR, LAMB2, MACROH2A1, NEXN, NOS3, PPM1F, PRKAA1, PSMD8, RPN1, RPS19, SFN, TNC, UBE2D1, UGDH
	WNT11	other	AKT1, ERBB3, ERK1/2, JUN, Mek, MTOR, Pkc(s), PRKCA, PTK2, RAF1, RHOA, ROCK, WNT11	0.447	1.32×10^{-6}	ACTB, AIP, C1QC, CAT, CD55, CNP, COL4A1, EIF6, EPRS1, GLS, GSK3B, GSR, NEXN, NOS3, PRKAR1A, ROCK1, RPS2, SEC22B, SOD1, TNC
	SNAI1	transcription regulator	Akt, CDH1, MUC1, SNAI1, SP1, TAFAZZIN, YAP1	0.471	3.02×10^{-6}	ACADSB, ACTB, ADD1, AEBP1, CAT, CD55, GSR, LAMB2, PSMD6, PSMD8, PYCR1, RANBP1, SOD1, STT3A, TNC, UGDH, UGP2, USP5
	ZEB2	transcription regulator	Akt, AKT1, ERK1/2, Nfat (family), P38 MAPK, PLCG2, RB1, ZEB2	1.414	1.03×10^{-5}	ACTB, ACTC1, ADD1, AIP, C1QC, CAT, CD55, CD9, COL4A1, FHL1, LAMB2, NDUFS2, NEXN, NOS3, PRKAR1A, SOD1, STT3A, TNC
	TWIST2	transcription regulator	TWIST2	0.577	1.53×10^{-3}	CAT, FBLN5, PRKAA1

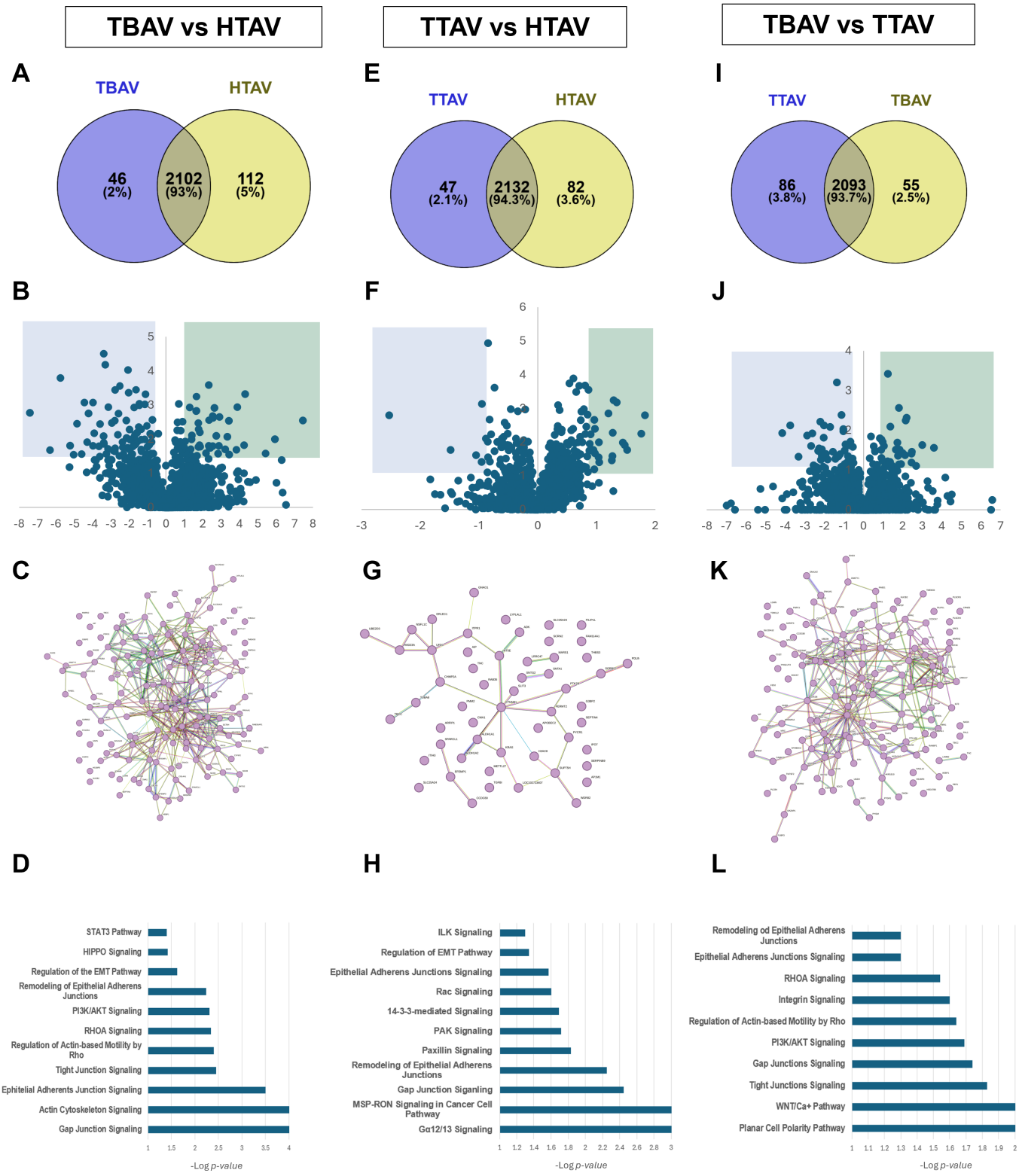

Figure 1. Quantitative proteomic analysis of the ascending aorta between experimental groups: TBAV vs. HTAV (**A**–**D**); TTAV vs. HTAV (**E**–**H**); and TBAV vs. TTAV (**I**–**L**). (**A**,**E**,**I**) Venn diagrams. (**B**,**F**,**J**) Volcano plots. (**C**,**G**,**K**) Protein-Protein interaction (PPI) network performed with String. Nodes represent proteins, and edges represent protein-protein associations. Significantly downregulated and upregulated proteins are labeled in blue and green boxes, respectively. (**D**,**H**,**L**) Canonical pathways identified by IPA based on protein alterations among experimental groups.

The GO terms are shown in Figure 2. The terms 'regulation of extracellular matrix organization' (p-value = 0.001053) and 'regulation of collagen fibril organization' (p-value = 0.001333) were among the top ten most significantly affected biological processes (Figure 2A). The molecular functions 'cadherin binding' (p-value = 0.00006378), 'oxidoreductase activity' (p-value = 0.0002594), 'protein phosphatase activator activity' (p-value = 0.0007174), 'nitric oxide synthase binding' (p-value = 0.001333) and 'MAP kinase kinase activity' (p-value = 0.006389) were significantly affected (Figure 2B). Regarding the cellular component terms, we found 'focal adhesions' (p-value = 0.00005157), 'cell-substrate adhesions' (p-value = 0.00006326), and 'elastic fibers' (p-value = 0.0003020) to be significantly affected (Figure 2C). All these GO terms are associated with the EMT process.

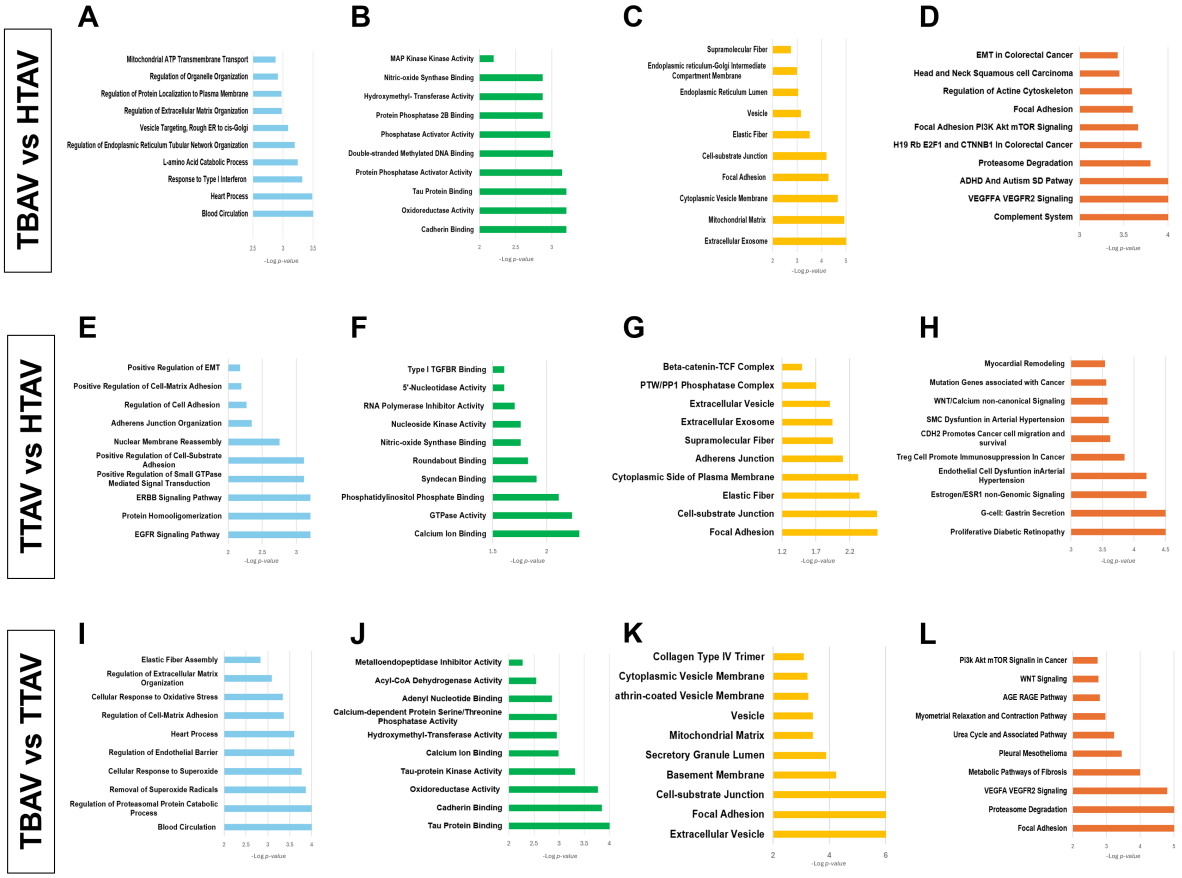

Figure 2. Enrichment analysis of differentially expressed proteins between experimental groups: TBAV vs. HTAV (**A**–**D**); TTAV vs. HTAV (**E**–**H**); and TBAV vs. TTAV (**I**–**L**). For each comparison, enrichment results are presented for Gene Ontology Biological Processes (**A**,**E**,**I**), Molecular Functions (**B**,**F**,**J**), Cellular Components (**C**,**G**,**K**), and Enrichr pathways from Wikipathway (**D**,**H**,**L**).

The Enrichr database Wikipathway also identified significant EMT-related terms (Figure 2D), including 'Epithelial to Mesenchymal Transition in Colorectal Cancer' (p-value = 0.0003) and 'TGFB Family in Epithelial to Mesenchymal Transition in Cancer' (p-value = 0.0005), with 14 proteins involved (TJP1, MAP2K4, VTN, MAP2K2, COL4A1, CTNNB1, KRAS, ROCK1, RHEB, EFEMP2, SGCD, SGCB, SLIT3, FBLN5). Similar to IPA causal network analysis, transcription factor enrichment analysis using the TTRUST Enrichr database identified SNAI1 and SNAI2 among the most significantly altered proteins (p-value = 0.002812 and p-value = 0.02294, respectively) (Table 2).

Table 2. Potential EMT regulators according to the TTRUST transcription factors database.

	Name	*p*-Value	Odds Ratio	Combined Score
HTAV vs. TBAV	TP53 human	0.002216	4.79	29.28
	HDAC1 human	0.002644	7.47	44.34
	PPARD human	0.002812	30.98	182.00
	SNAI2 mouse	0.002812	30.98	182.00
	YY1 human	0.006422	5.75	29.01
	SNAI1 mouse	0.02294	9.17	34.62
HTAV vs. TTAV	LEF1 human	0.002382	30.75	185.70
	SOX4 mouse	0.01491	81.41	342.39
	SOX6 human	0.01491	81.41	342.39
	ZBTB33 mouse	0.01491	81.41	342.39
	VDR mouse	0.01983	58.14	227.95
	TFAP2A mouse	0.02473	45.22	167.30
	SNAI2 mouse	0.02473	45.22	167.30
TTAV vs. TBAV	TFCP2 human	0.001892	38.84	243.49
	PPARD human	0.002354	33.98	205.63
	NFE2L2 human	0.006098	19.41	98.99
	TWIST2 mouse	0.04359	27.00	84.60

The interactome of proteins specifically detected in EMT terms from IPA canonical pathways and GO terms showed a significant PPI enrichment, indicating clear interactions among this pool of proteins (p-value = 0.0347) (Figure 3C). A new GO term analysis for these proteins pointed to terms such as 'cell adhesion' (p-value = 0.0057), 'cell-matrix adhesion' (p-value = 0.0490), 'anatomical structure morphogenesis' (p-value = 0.0136), and 'cell development' (p-value = 0.0471) (Figure 3D).

Finally, an interactome analysis was performed, including proteins provided by terms that specifically contained 'EMT' from the IPA canonical pathways and GO term enrichment analyses. These proteins interact significantly (p-value = 0.000149) according to the STRING database (Figure 3A), and the most significant GO biological processes were mainly related to developmental events, including 'muscle cell differentiation' (p-value = 9.98×10^{-5}), 'circulatory system development' (p-value = 1.17×10^{-5}), 'heart development' (p-value = 0.00012) and 'smooth muscle cell differentiation' (p-value = 0.0027) (Figure 3B).

3.1.2. TTAV vs. HTAV

The TTAV vs. HTAV comparison showed 2132 total proteins in the ascending aorta, 55 of which were differentially expressed (25 up- and 30 down-regulated in TTAV specimens, Figure 1E,F and Table S4) and had a significant PPI enrichment in the STRING database (p-value = 0.0362) (Figure 1G). The IPA analysis of canonical pathways showed 66 enriched pathways (Table S5). These IPA pathways fit the same ten categories mentioned in the TBAV vs. HTAV comparison, including the Developmental and cell fate pathways that contained the term 'Regulation of the Epithelial–Mesenchymal Transition Pathway' (p-value = 0.038), with two related proteins (CTNNB1 and KRAS). Additionally, we found 12 pathways directly associated with the EMT process (Figure 1H). Furthermore, SOX2-OCT4-NANOG, LATS2, SOX2, ZEB, and SOX1 (p-values of 3.40×10^{-5}, 5.05×10^{-5}, 8.79×10^{-5}, 1.15×10^{-4},

and 5.08×10^{-3}, respectively) emerged as altered EMT regulatory factors in the IPA causal network analysis (Table 1).

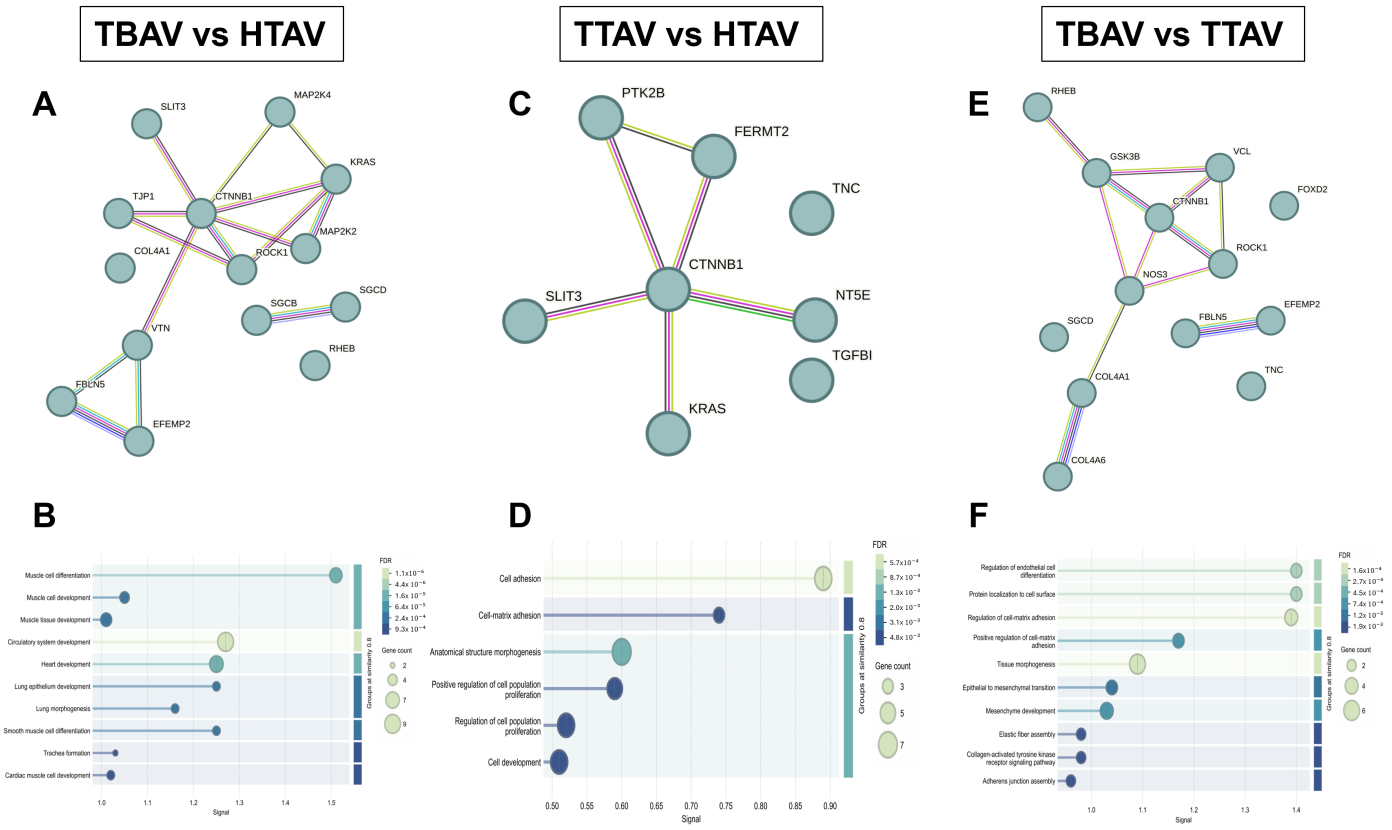

Figure 3. Protein-protein interaction networks of differentially expressed proteins identified in EMT terms by Enrichr in the three comparisons: TBAV vs. HTAV (**A**,**B**); TTAV vs. HTAV (**C**,**D**); and TBAV vs. TTAV (**E**,**F**). (**A**,**C**,**E**) Protein–protein interaction networks. Nodes represent proteins, and edges represent experimentally validated or predicted functional interactions. (**B**,**D**,**F**) Gene Ontology biological processes significantly enriched in the EMT-associated protein sets. Bar plots show the most significantly enriched biological processes ranked according to enrichment significance. The circles size indicates the number of proteins in the dataset that are involved.

Regarding GO terms enrichment, most of the significant top ten biological processes were related to EMT: 'epidermal growth factor receptor signaling pathway' (p-value = 0.0003154), 'ERBB signaling pathway' (p-value = 0.0005012), 'positive regulation of Cell-Substrate Adhesion' (p-value = 0.0007766), 'adherens junction organization' (p-value = 0.004496), 'regulation of cell adhesion' (p-value = 0.005382), 'positive regulation of cell-matrix adhesion' (p-value = 0.006420), and 'positive regulation of epithelial to mesenchymal transition' (p-value = 0.006683) (Figure 2E). The last term specifically quotes EMT and involved eight proteins (CTNNB1, NT5E, TNC, SLIT3, TGFBI, FERMT2, KRAS, PTK2B). The significantly altered molecular functions identified by GO term enrichment were also related to EMT: 'syndecan binding' (p-value = 0.01244), 'roundabout binding' (p-value = 0.01491), 'nitric-oxide Synthase binding' (p-value = 0.01737), and 'type I transforming growth factor beta receptor binding' (p-value = 0.02473) (Figure 2F). With regard to the cellular components, 'focal adhesion' (p-value = 0.002284), 'cell-substrate junction' (p-value = 0.002505), 'elastic fiber' (p-value = 0.004496), 'adheren junction' (p-value = 0.008002), and 'beta-catenin-TCF complex' (p-value = 0.03203) were the emerged terms (Figure 2G).

When we performed the analysis with the Enrichr database, 'endothelial cell dysfunction in arterial hypertension' (p-value = 0.00006929), 'smooth muscle cell dysfunction

in arterial hypertension' (p-value = 0.0002653), 'WNT/calcium non-canonical signaling' (p-value = 0.0002721), and 'myocardial remodeling' (p-value = 0.0002813) arose as significantly altered (Figure 2H). While WNT signaling is a direct regulator of EMT, the remodeling process associated with arterial hypertension and myocardial fibrosis has been shown to involve EMT [33]. In the TTRUST transcription factors database, we found LEF1, SOX4, SOX6, ZBTB33, VDR, TFAP2A, and SNAI2 as the most probable regulators of EMT affected in the aorta of TTAV animals (p-values = 0.002382, 0.01491, 0.01491, 0.01491, 0.01983, 0.02473, and 0.02473, respectively) (Table 2).

3.1.3. TBAV vs. TTAV

The last comparison, TBAV vs. TTAV, revealed a total of 2093 proteins, 182 of them significantly altered (90 up- and 92 down-regulated) in the aorta of TBAV animals (Figure 1I,J) and Table S6, with a significant PPI enrichment that demonstrates non-random interactions (p-value = 7.85×10^{-9}) (Figure 1K). In this case, IPA identified 126 canonical pathways significantly enriched (Table S7) that matched the ten general categories previously established. In the Developmental and cell fate pathways category, we found pathways such as WNT/Ca+ pathway (p-value = 0.0048977), Semaphorin Neuronal Repulsive Signaling Pathway (p-value = 0.043651), and PCP (Planar Cell Polarity) Pathway (p-value = 0.0038019), which are terms related to EMT. In total, 16 out of the 126 enriched canonical pathways were associated with EMT, including the PI3K-AKT pathway (Figure 1L). The IPA causal networks showed ZEB1, TWIST, WNT11, SNAI1, ZEB2, and TWIST2 as potential regulators of EMT affected in TBAV animals (p-values = 1.33×10^{-9}, 1.23×10^{-7}, 1.32×10^{-6}, 3.02×10^{-6}, 1.03×10^{-5}, and 1.53×10^{-3}, respectively) (Table 1).

The enrichment analysis for GO terms revealed 'removal of superoxide radicals' (p-value = 0.0001361), 'regulation of establishment of endothelial barrier' (p-value = 0.0002502), 'positive regulation of cell-matrix adhesion' (p-value = 0.0004350), 'cellular response to oxidative stress' (p-value = 0.0004518), 'regulation of collagen fibers organization' (p-value = 0.001115), and 'elastic fiber assembly' (p-value = 0.001479) as the most significant biological processes (Figure 2I). For molecular functions, we detected significant terms such as 'cadherin binding' (p-value = 0.0001424), 'oxireductase activity' (p-value = 0.0001704), 'calcium binding' (p-value = 0.001030), and 'metalloendopeptidase inhibitor activity' (p-value = 0.005361) (Figure 2J). According to cellular components, 'focal adhesion' (p-value = 3.086×10^{-10}), 'cell-substrate junction' (p-value = 4.348×10^{-10}), 'basement membrane' (p-value = 0.00005845), and 'collagen IV type trimer' (p-value = 0.0008001) were significantly enriched, among others (Figure 2K).

When we checked the Enrichr database (Figure 2L), three pathway terms that explicitly included EMT emerged as significantly altered (Table S8): 'Epithelial to Mesenchymal Transition in Colorectal Cancer' (p-value = 0.03122), 'Epithelial to Mesenchymal Transition in Cancer: Overview' (p-value = 0.029) and 'WNT in Epithelial to Mesenchymal Transition in Cancer' (p-value = 0.040), with 13 proteins included (FOXD2, EFEMP2, NOS3, COL4A6, COL4A1, CTNNB1, GSK3B, ROCK1, RHEB, SGCD, FBLN5, TNC, VCL). The TTRUST transcription factor database showed TFCP2, PPARD, NFE2L2, DDIT3, and TWIST as candidates for EMT regulators (p-values = 0.001892, 0.002354, 0.006098, 0.007700, and 0.04359, respectively) (Table 2).

Regarding the interactome for EMT terms that were specifically detected in the Enrichr database, we found significant interaction among the proteins involved, with a PPI enrichment p-value = 0.000763 (Figure 3E). The GO term analysis for this set of proteins showed terms such as 'regulation of endothelial cell differentiation' (p-value = 0.0065), 'tissue morphogenesis' (p-value = 0.0065), 'epithelial to mesenchymal transition' (p-value = 0.0158) and 'mesenchyme development' (p-value = 0.0158) (Figure 3F).

3.2. EndMT During Murine OFT Septation

Figure 4 shows the septation of the middle cardiac OFT in the mouse embryo. In the OFT of E11.5 embryos, conal ridges (CRs) appear as two long independent cushions composed of cardiac jelly, mesenchymal cells and a lining endocardium (Figure 4A–C). The distal portion of the CRs, corresponding to the middle OFT, constitutes the primordia of the aortic and pulmonary roots. Mesenchymal cells in the core of CRs are mainly derived from EndMT, CNC and second heart field (SHF) cells [10]. The fusion event begins between E11 and E11.5, when the endocardia lining the most distal portion of the CRs come into contact (Figure 4C(C′)) and disappear (Figure 4D(D′)), enabling the two mesenchymal cores to become continuous, and the CNC cells to form the conal septum (Figure 4C(C′),D(D′)). The fusion occurs progressively from the middle to the proximal OFT (Figure 4A) until E12.5. At this stage, the CNC-derived mesenchymal cells of the conal septum aggregate at the center of the fused CRs, while OFT myocardial cells migrate to form the infundibular OFT (Figure 4E(E′)). The whole process is summarized in Figure 4F.

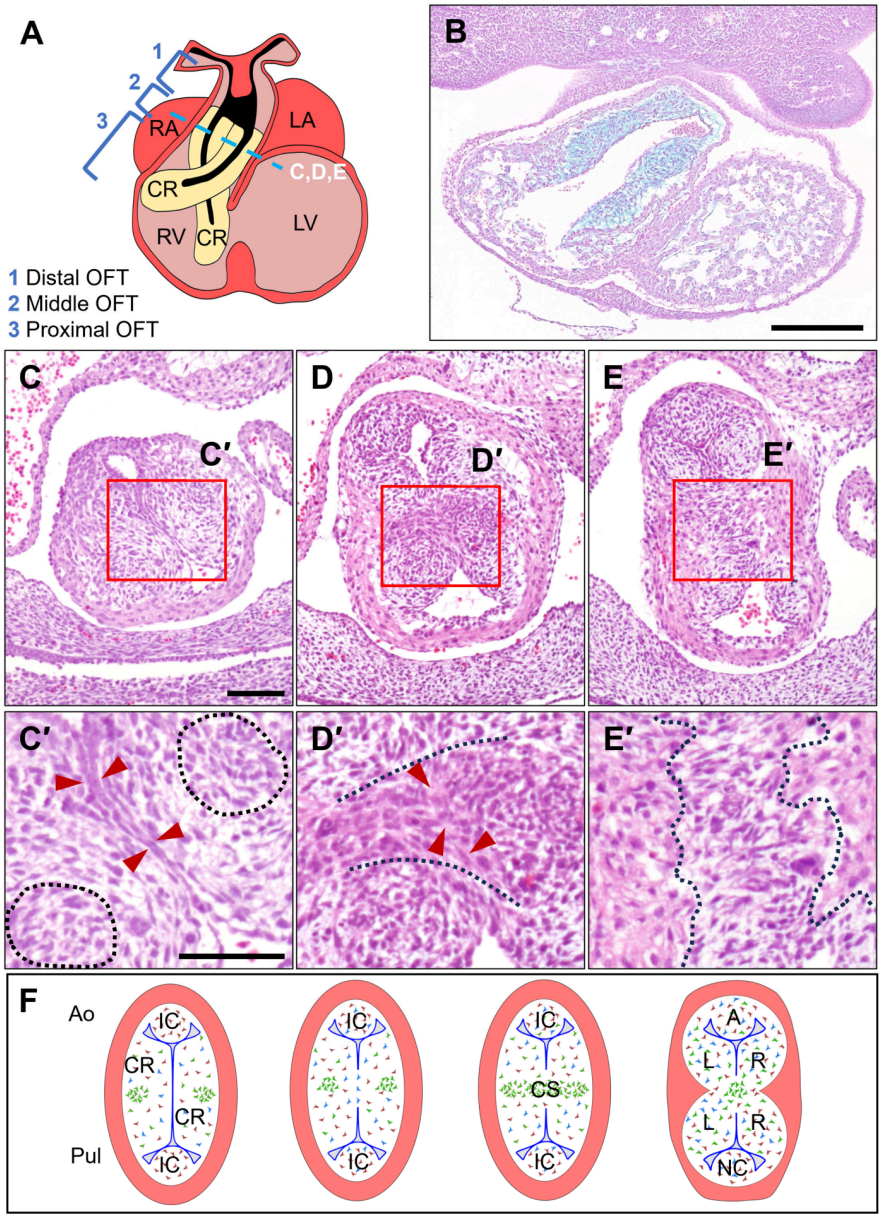

Figure 4. Septation of the cardiac OFT in the mouse. (**A**,**B**): Schematic representation (**A**) and histological section stained with Alcian blue-Fast red (**B**) of a mouse embryonic heart at E11.5 in frontal

view. Conal ridges (CRs) are shown along the OFT (with cardiac jelly strongly stained in blue in (**B**)), together with the aortic-pulmonary septation complex (black in (**A**)), composed of CNC cells that take on an inverted-U shape. (**C**–**E**,**C′**–**E′**): Transverse sections of E11.5 (**C**,**D**,**C′**,**D′**) and E12.5 (**E**,**E′**) embryonic hearts stained with Hematoxylin-Eosin show the septation of the distal CRs, i.e., at the middle portion of the OFT (2 in (**A**)). At E11.5, the central region of the two opposite CRs comes into contact (**C**,**C′**) and fuses (**D**,**D′**). At E12.5, the conal septum (CS) is formed between the semilunar valve primordia (**E**,**E′**). Red squares in (**C**–**E**) show magnifications of the fusion area in consecutive transverse sections (**C′**–**E′**). Arrowheads indicate endocardial cells in contact (**C′**) and transformed (mesenchymal) cells (**D′**). Dotted lines indicate the boundary of the CNC cells (**C′**,**D′**) and the conal septum (**D′**,**E′**). (**F**): Schematic representation of transverse views of the middle OFT that represent consecutive stages of the septation process. During normal fusion of the CR, endocardial cells transform into mesenchymal cells through EndMT (blue). Parallelly, CNC cells (green), initially distributed in prongs, migrate to the central portion of the CR to form the CS. SHF-derived cells (red) distribute throughout the outflow cushions, forming most of the intercalated cushions (IC). The CS divides the distal conus into two aortic (Ao) and pulmonary (Pul) independent OFTs, each containing three valve cushions. A: anterior intercalated cushion; L: left aortic or pulmonary valve cushion; LA: left atrium; LV: left ventricle; NC: non-coronary intercalated cushion; R: right aortic or pulmonary valve cushion; RA: right atrium; RV: right ventricle. Scale bars: 250 μm in (**B**), 100 μm in (**C**–**E**), 50 μm in (**C′**–**E′**).

A previous study performed in hamster embryos allowed us to raise the hypothesis that fusion of endocardial cushions during OFT septation relies on a process of EndMT localized at the center of the CRs (Figure 4F) [25]. NOTCH1 is a well-known key regulator of EndMT at earlier cardiogenetic stages, during the formation of the endocardial cushions in the OFT and the atrioventricular canal [34]. In addition, Notch1 transgenic mice have been demonstrated to develop AP-BAV [35]. We hypothesized that re-activation of this signaling pathway in the endocardium of the distal CRs could lead to the fusion of CRs that occurs in the septation process. We performed triple immunofluorescence for the endocardial marker ETS transcription factor (ERG), the intracellular domain of NOTCH1 (N1ICD) as a central EndMT-regulating transcription factor, and α-smooth muscle actin (SMA) as a myocardial and migratory mesenchymal marker in OFTs of E11.5 mouse embryos. ERG was expressed in the nuclei of all the endocardial cells of the embryonic heart, including the lining endocardium of the CRs (Figure 5A,B). When we inspected the expression of N1ICD, we found that it was also expressed in the nuclei of endocardial cells. However, its location was restricted to the endocardium covering the ventricular trabeculae and parts of the OFT (Figure 5A,B). A sharp limit was found between $ERG^+;N1ICD^+$ trabecular endocardium and $ERG^+;N1ICD^-$ CR endocardium (arrows in Figure 5A(I–I″)). N1ICD endocardial signals in the OFT were restricted to the distal portion of the CR (Figure 5A(I,I″)). In those sections where fusing endocardia were identified, opposing endocardia covering the CR were $ERG^+;N1ICD^+$ (yellow bracket in Figure 5B(II,II″)), while endocardial cells just proximal to the area of fusion were $ERG^+;N1ICD^-$ (white bracket in Figure 5B(II,II″)). When the area of fusion was explored in detail (Figure 5B(III–III‴)), we observed that cells lose ERG expression, gain a-SMA staining, and acquire a mesenchymal phenotype. Moreover, while ERG^+ endocardial cells adjacent to the area of fusion showed strong N1ICD staining, ERG^- mesenchymal cells in the area of fusion showed weak N1ICD signals. We interpret these results as downregulation of N1ICD after EndMT, as previously described [35].

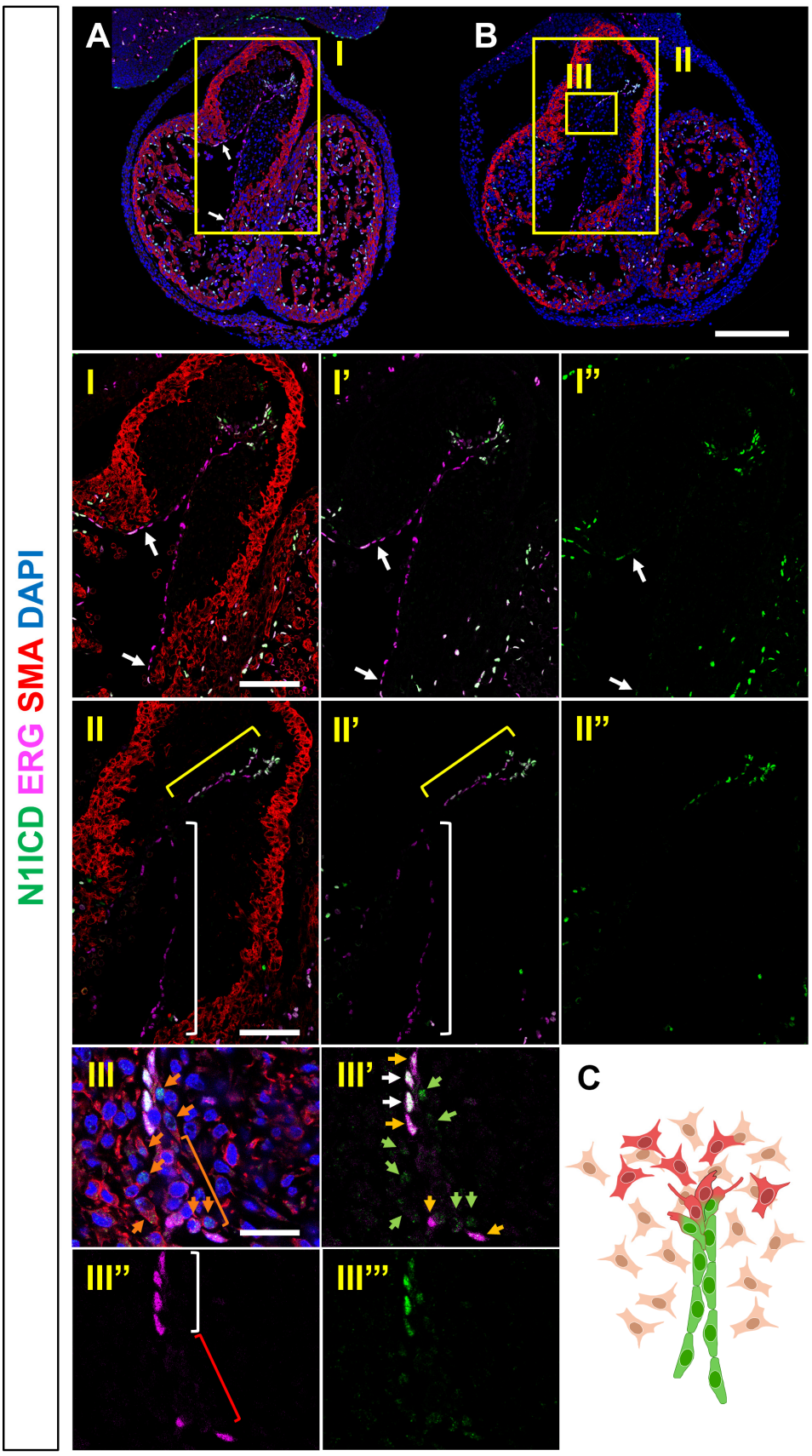

Figure 5. Immunofluorescence for endocardial (ERG), EndMT (N1ICD), mesenchymal migration and myocardium (SMA) markers in frontal (**A**,**B**) histological sections of the proximal and middle

OFT of E11.5 mouse embryos. Yellow rectangles show magnifications of the OFT for (**A**) in (**I–I″**) and for (**B**) in (**II–III‴**). White arrows in (**A**) and (**I–I‴**) point to the limit between ERG$^+$;N1ICD$^-$ endocardial cells from CRs and ERG$^+$;N1ICD$^+$ endocardial cells from myocardial trabeculae. The yellow bracket in (**II**,**II′**) frames the endocardium covering the two CRs during the process of fusion (ERG$^+$;N1ICD$^+$), while the white bracket corresponds to the endocardium of the proximal portion of the CRs, far from the fusion area (ERG$^+$;N1ICD$^-$). The orange bracket in (**III**,**III″**) shows the oblique fusion area, where orange arrows point to ERG$^-$;N1ICD$^+$;SMA$^+$ cells undergoing EndMT. In (**III′**), white arrows point to ERG$^+$; strong N1ICD$^+$ endocardial cells, yellow arrows to ERG$^+$; weak N1ICD$^+$ endocardial cells that are ready to transform, and green arrows to ERG$^-$; weak N1ICD$^+$ mesenchymal cells near the fusion area, indicating mesenchymal cells provided by recent EndMT. The white bracket in (**III″**) shows ERG$^+$ endocardial cells outside the fusion area, while the red bracket frames ERG$^-$ endocardial cells in the fusion area. In (**C**), a diagram of the sequential EndMT process that occurs during the fusion of CRs is shown in frontal view. Green cells are quiescent endocardial cells located proximally in the OFT; green-red cells are endocardial cells transforming into mesenchyme in the middle portion; and red cells are EndMT-derived mesenchymal cells. Brown cells are mesenchymal cells that form the core of CRs. Diagram reprinted with permission [25]. Scale bars: 200 μm in (**A**,**B**), 100 μm in (**I–II″**), 25 μm in (**III–III‴**).

4. Discussion

The so-called 'fetal gene hypothesis' was proposed almost 40 years ago, referring to the reactivation of embryonic gene programs in the adult heart in response to stress [36]. [17]. The etiology of BAV aortopathy has been proposed to be explained by the fetal gene hypothesis [14,21–23]. Given that EndMT is responsible for aortic valve primordia formation [31,37], it was proposed that this cellular mechanism may be the link between the embryonic valve defect and the early phases of the adult AD [14,21–23]. However, there is currently no direct experimental evidence of EndMT alterations during BAV formation, which could be reactivated in the adult aorta to initiate AD. Likewise, evidence of EndMT involvement in human adult aortopathy does not allow formulating a coherent mechanistic hypothesis of disease development.

In this manuscript, we present consistent molecular evidence suggesting the involvement of EndMT in the early phase of AD in the BAV hamster model, in which aortic valve malformation relies on alterations of EndMT during embryonic OFT septation [25]. The finding of a link between aortic valve development and adult aortopathy initiation in the same animal model provides strong proof for the fetal gene hypothesis in the etiology of BAV disease. In addition, we present morpho-molecular evidence for the participation of EndMT in the murine OFT septation process (particularly in the fusion of the distal CRs that forms the valve primordia), reinforcing our hypothesis and extending the extrapolability of our results.

4.1. EndMT in BAV Embryonic Development

Several rodent models have shown that the two anatomical types of BAV, latero-lateral (LL) and antero-posterior (AP) BAVs, rely in most cases on alterations in two distinct morphogenetic mechanisms: endocardial cushion formation and OFT septation, respectively [31].

Early in valvulogenesis, a population of CNC- and SHF-derived cells from the circumpharyngeal region invade the pericardial cavity through the embryonic distal OFT [38–40]. There, a CNC-specific developmental program induces EndMT in the endocardium, which in turn regulates CNC migration through the middle and proximal OFT [41]. SHF- and CNC-derived cells subsequently form the walls of the aortic and pulmonary trunk primordia and, along with endocardial-derived cells, contribute to the distal CRs, the primordia of the

aortic and pulmonary valves [10,11,42]. Later in development, CNC cells induce localized fusion of the two CRs and build the transient CS, which subsequently regresses through apoptosis of septal CNC mesenchymal cells [25,43–45] (Figure 4). This process, termed OFT septation, divides the middle and proximal OFT symmetrically and leads to the formation of the OFT valve primordia [42,46]. Therefore, the developmental program of CNC in the embryonic OFT involved in arterial formation, septation, and valve morphogenesis includes induction of EndMT, migration, and apoptosis.

Embryonic studies in transgenic mouse models have shown that abnormal CNC migration, CNC-SHF interactions, and/or defective EndMT are responsible for alterations in OFT endocardial cushion formation that may result in LL-BAVs [31]. The development of AP-BAV, the most common BAV anatomical type in patients [2,5], hamsters [24–32], and *Notch1* transgenic mice [35], occurs later, during OFT septation due to extra-fusion of the distal CRs (Figure 6). The cellular mechanism responsible for the fusion of the CRs was recently uncovered in the hamster model. Soto-Navarrete et al. [25] found consistent morphological evidence of EndMT in the process of fusion and extra-fusion of the distal CR in hamsters, which leads to TAV and AP-BAV formation, respectively (see Figures 4F and 6). These data suggest that both LL- and AP-BAVs may result from alterations of the same cellular process (EndMT) at two different developmental time points [25,31]. However, the involvement of EndMT in OFT septation has not been reported in the murine model, limiting the extrapolability of the results and the consistency of the hypothesis.

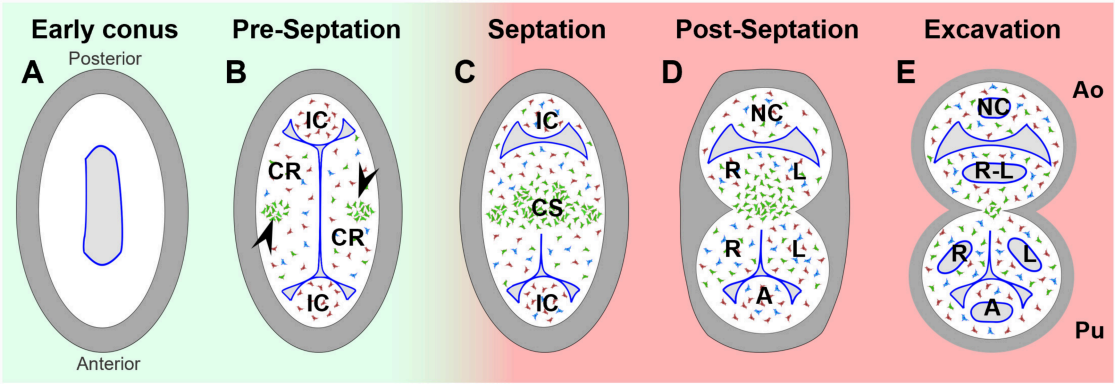

Figure 6. Schematic representation showing transverse views of the middle OFT during abnormal septation leading to antero-posterior (AP-) BAV (**A**–**E**). In the hamster model with AP-BAV, cellularization of the cardiac jelly looks normal (**B**), but abnormal fusion and a defective conal septum (CS) result in an AP-bicuspid valve anatomy (**C**–**E**). The proportion of mesenchymal cells from each embryonic lineage (CNC in green, SHF in red and endocardial-derived in blue) in the OFT cushions is represented according to [10]. The real distribution of lineage-specific mesenchymal cells is shown only for the CS. But it does not reflect the fine morphology or the state of differentiation in all the stages shown. Black arrowheads indicate prongs of CNC cells prior to CS formation. Modified from [31]. Reprinted with permission.

In the present study, we have inspected the process of fusion of the distal CRs in the mouse model, using serial histological sections and immunofluorescence against endocardial (ERG), mesenchymal (SMA), and EndMT (N1ICD) molecular markers. The analysis showed similar morphologic results to those obtained in the hamster model [25]. First, the endocardial cells of opposing distal CRs come into contact and disappear, allowing the formation of a mesenchymal conal septum, which is later replaced by myocardial cells (Figure 4). Immunofluorescence with endocardial (ERG) and EndMT (N1ICD) markers showed that those cells that delineate the area of fusion lose the endocardial morphology and endocardial markers (ERG; Figure 5), acquiring a mesenchymal (a-SMA$^+$; Figure 5)

phenotype. In addition, we found ERG and N1ICD double labeling specifically in the endocardial cells adjacent to the area of fusion of the CRs, while mesenchymal cells in the area of fusion consistently showed weak N1ICD staining (Figure 5). We interpret these results as an ongoing process of EndMT, specifically localized at the endocardium covering the center of the opposing CRs. These endocardial cells express N1ICD, activate EndMT and induce loss of endocardial markers to acquire a mesenchymal phenotype.

The NOTCH1 molecular pathway is a well-known regulator of the EndMT process responsible for CR formation [34,35]. In the murine embryonic heart, N1ICD is expressed in the whole endocardium of the OFT at E10.5, activating EndMT to populate the core of the CRs with mesenchymal cells [35]. Our results indicate that this pathway is reactivated at E11.5, during OFT septation, specifically in the area of fusion of the CRs. NOTCH1 is a transmembrane receptor that, after activation by ligands such as JAG1 or DLL4 and proteolytic cleavage, has its NOTCH1 intracellular domain excised and translocates to the nucleus to activate transcription of EndMT-specific genes [47]. Once the endocardial cells have been transformed, the resulting mesenchymal cells downregulate NOTCH1 [34,35]. We found strong evidence that this pattern of NOTCH1 expression, nuclear translocation and final downregulation is replicated during OFT septation, specifically in the area of fusion of the CRs (Figure 5). These results indicate that the endocardial NOTCH signaling pathway is likely the main EndMT activator linked spatially and temporally with the process of fusion of the CRs during OFT septation.

The specific expression of N1ICD in the distal portion of CRs especially caught our attention given the proximity of CNC cells and their role in cardiac OFT septation [41,45,48]. These cells form an inverted U-shaped structure called the aortic-pulmonary septation complex (Figure 4A), which progresses disto-proximally along the CRs to promote the fusion event [41,42,45,48]. The present set of results obtained in the mouse model, together with our previous morphological, molecular and morpho-molecular evidence obtained in the hamster model [25], reinforces the hypothesis that CNC cells induce a complete EndMT process specifically in the endocardium covering the central portion of the CRs, mediated by the NOTCH signaling pathway, to promote cardiac OFT septation. Previous studies have shown that during cardiogenesis, JAG1 is specifically expressed by CNC cells and is also related to BAV formation [35,49]. JAG1 is also a transmembrane receptor, so NOTCH1 activation by JAG1 relies on cell-cell contact [47]. Importantly, our previous studies in the hamster model showed that the extension of the fusion of the CRs leading to AP-BAV formation is spatially associated with excessive migration of CNC cells involved in OFT septation (Figure 6) [24,31,50]. This, together with the fact that mutations in *Notch1* have been associated with BAV in both patients and genetically modified mouse models [35,51], allows us to hypothesize that the underlying cause of BAV lies in abnormally migrating CNC cells that over-induce EndMT through N1ICD activation in endocardial cells, extending the fusion area of CRs involved in cardiac OFT septation. However, we cannot discard a possible additional involvement of SHF-derived cells of the CRs in the fusion process. Cell lineage tracing in appropriate transgenic mouse models may solve this issue.

4.2. EndMT in BAV Aortopathy

EndMT has been suggested as a mechanism that may trigger ascending aortic degeneration in patients with BAV [14,15,20–23], specifically by studies mainly based on -omic technologies [14,15,20,21,23]. Interestingly, enrichment analysis of patient proteomic datasets confirmed the presence of deregulated pathways associated specifically with both embryonic EndMT and migration of CNC cells [21,22]. In addition, experimental evidence using human induced pluripotent stem cells has shown defective differentiation of CNC-derived SMCs in BAV patients [12]. However, the heterogeneous nature of patient

populations (i.e., patient cohorts with different clinical presentations and disease etiologies) has made it impossible to corroborate the involvement of EndMT, CNC-derived SMCs, and the origin of the initial stimulus (genetic defects and/or hemodynamic factors related to BAV morphology).

The spontaneous BAV hamster model (T strain) has been demonstrated to be suitable for studying BAV syndrome due to its high similarity to human disease [28,30], thereby resulting in a high extrapolation capacity [2,24,30–32,37,52,53]. In fact, T strain animals present with non-aneurysmal ascending AD, independently of the valve morphology, exhibiting histopathological and molecular alterations analogous to those observed in patients [26].

Animals from the T strain are genetically and phenotypically homogeneous, which means that, as compared with patient cohorts, this inbred isogenic hamster population exhibits a high incidence of exclusively AP-BAV (~40%) together with fully penetrant AD, with a specific etiology [24–32]. This is a major advantage for two main reasons. Firstly, this homogeneity allows for more consistent results compared with those obtained in heterogeneous patient populations. Secondly, the characteristics of the model make it possible to distinguish between genetic and hemodynamic factors when three experimental groups are compared. Therefore, our analysis strategy is based on the following group comparisons: (1) TBAV vs. HTAV (genetic + hemodynamic factors), with different genetic background and valve morphology, let hemodynamics and genetic factors emerge; (2) TBAV vs. TTAV (hemodynamic factors), with the same genetic background but different valve morphology due to reduced penetrance of the trait (caused by epigenetic and environmental factors such as embryonic stochastic variations [54]) allow to study the hemodynamic component exclusively; and (3) TTAV vs. HTAV (genetic factors), with different genetic background but normal valve morphology, which have been demonstrated to be virtually the same in both strains [32], can separate only genetic factors. This experimental strategy was the basis for the interpretation of the proteome reanalysis.

4.2.1. The Hamster Aortic Proteome Reanalysis

In a recent comparative proteomic study in the hamster model [27], our group applied a rigorous data analysis strategy, selecting only the proteins that exhibited concordant differential expression in the three replica samples analyzed. This strategy aimed to obtain stringent results for the validation of the hamster T strain as an animal model of BAV aortopathy, and to compare the central molecular factors operating in the hamster aorta with those previously described in affected patients. Two molecular pathways emerged as the most consistent: the WNT/β-catenin and the PI3K-AKT pathways. The WNT/β-catenin pathway emerged as the major genetic factor contributing to BAV disease. It is one of the main intracellular regulators of EndMT involved in endothelial cell detachment and regulation of EMT-specific gene expression [55]. Although this signaling pathway has been reported in human aortopathy initiation and progression [15,56,57], little is known about its specific role in AD. The PI3K-AKT pathway appeared as a central regulator, triggered by hemodynamic factors, of a common assemblage of interconnected altered pathways, including Wnt/β-catenin. PI3K/AKT [58,59] has been previously associated with SMC phenotype shift (i.e., the reversible change from a differentiated, quiescent, contractile state toward a more synthetic, proliferative, migratory state in response to environmental cues [60]) in patients with BAV aortopathy [61]. However, it is worth mentioning that it also regulates EMT in development, fibrosis, and cancer [58,59]. Although in our previous IPA analysis, the term 'Regulation of the Endothelial to Mesenchymal Transition' was identified in 'Canonical pathways', it did not reach a sufficient level of significance

($-\log(p\text{-value}) = 1.21$; $p\text{-value} = 0.061$). Consequently, this particular term was excluded from further investigation, and the discussion was focused on SMC phenotype shift.

In the present study, we have reassessed these proteomic data with a less stringent strategy, incorporating differentially expressed proteins found in two out of the three replicates. Then we performed an enrichment analysis using IPA software (Qiagen, Inc., 2024) (canonical pathways), interactomes (STRING database), GO terms, and Enrichr databases (Wikipathway). Interestingly, the new reanalysis revealed specific terms for EMT in all comparisons (Figures 1 and 2), suggesting a specific role for this cellular process in AD etiology. Overall, we found alterations in the same central pathways as those identified in our previous results [27], including the WNT/β-catenin and PI3K-AKT pathways. However, in the first study, the alterations in PI3K-AKT signaling were exclusively detected in the TBAV vs. HTAV comparison. Now, we detected this dysregulation also in the TTAV vs. TBAV comparison, reinforcing the idea that this difference in the aortic proteome most likely relies on hemodynamics. Regarding the WNT pathway, it was originally detected in the TTAV vs. HTAV comparison, suggesting a genetic etiology. In the new reassessment, this pathway was additionally detected in the TTAV vs. TBAV comparison, suggesting a hemodynamic influence. Given that the WNT/β-catenin pathway can be regulated by the PI3K-AKT signaling [62], this reanalysis alerts to a possible genetic defect associated with the WNT pathway in animals from the T strain, irrespective of the aortic valve morphology, that alters the structural stability of the ascending aorta, likely through induction of EndMT, which is probably exacerbated by the defective regulation of PI3K-AKT caused by hemodynamics in those specimens carrying a BAV [27].

4.2.2. The EndMT Interactome Analysis

We performed an additional interactome analysis (STRING database) for differentially expressed proteins included specifically in EMT terms (Figure 3). The TBAV vs. HTAV comparison would be expected to uncover the highest number of differentially expressed proteins because it accounts for both hemodynamic and genetic factors. Also for this reason, a significant proportion of differentially expressed proteins would be expected to be common among comparisons. Fourteen EndMT-associated proteins were found dysregulated between TBAV and HTAV aortas, while the TBAV vs. TTAV and the TTAV vs. HTAV comparisons revealed 11 and 7 dysregulated proteins, respectively (Figure 3). Nine out of the 14 proteins identified in TBAV vs. HTAV were also dysregulated in other comparisons. Remarkably, CTNNB1 (β-catenin) was the only protein differentially expressed in the three comparisons, suggesting both genetic and hemodynamic triggering. Given that CTNNB1 is the main effector of the WNT pathway, this finding reinforces the idea of an existing link between a congenital defect of the WNT/β-catenin pathway and the hemodynamic alteration of PI3K-AKT modulated by the presence of a BAV. As mentioned before, WNT/β-catenin and PI3K-AKT signaling are known to be involved in EMT regulation [55,58]. Taken together, these findings support that both pathways are the main candidates to trigger EndMT in the aorta of TTAV and TBAV hamsters. Six additional proteins were found differentially expressed in the TTAV vs. HTAV comparison. CTNNB1, KRAS and SLIT3 were also found to be quantitatively altered in the TBAV vs. HTAV comparison. Therefore, these three proteins are the most consistent candidates to be involved in the genetic predisposition of the aorta of T strain hamsters. The KRAS-MEK-ERK pathway is known to regulate the EMT process associated with CNC cell detachment from the neural tube before migration, during early embryonic stages [63,64]. The SLIT-ROBO pathway influences the proliferation, delamination, and migration of CNC cells, with SLIT3 strongly implicated in the migration process [65,66]. When CNC cells reach the embryonic heart, the WNT pathway regulates the migration of CNC cells into the embryonic OFT [67], and the EndMT

process associated with endocardial cushion formation [55,68]. Some of these CNC cells will differentiate into SMCs of the ascending aorta [11]. Therefore, the alteration of KRAS, SLIT3, and CTNNB1 suggests a genetic defect in T strain animals that probably affects first the EMT required for CNC detachment and the subsequent migration during OFT formation and septation. This is likely to impair the differentiation and behavior of SMCs, promoting a structural defect in the adult ascending aorta of TTAV and TBAV hamsters.

The TBAV vs. TTAV comparison identified quantitative alterations in a total of 11 EndMT-associated proteins, seven of which were also found dysregulated in the TBAV vs. HTAV comparison: CTNNB1, ROCK1, RHEB, EFEMP2, FBN5, COL4A1, and SGCD. These proteins are the most consistent candidates to be altered by hemodynamics in hamster BAV aortas. CTNNB1, ROCK1, and RHEB can be placed downstream of PI3K-AKT signaling. AKT can increase β-catenin transcriptional activity and its nuclear localization [62], suggesting that PI3K-AKT may be the flow-sensitive pathway that converts a genetically primed WNT state into active β-catenin-dependent transcription, promoting the expression of EndMT-related genes. On the other hand, PI3K-AKT signaling through ROCK1 has a strong connection with mechanical stress, by regulating actomyosin contractility, focal adhesions, cell stiffness, migration, and cytoskeletal tension [69]. Thus, it can act in both endothelial and smooth muscle cells [70], changing cell shape and junctional tension in the aortic endothelium for EndMT or promoting a phenotypic shift from contractile to synthetic in SMCs. RHEB is a direct activator of mTOR, a signaling pathway downstream of PI3K-AKT [71]. Alterations in RHEB-mTOR promote SMC phenotypic switch [12]. Hence, RHEB is a plausible hemodynamic effector that acts in SMCs, but it is not necessarily an initiator of EndMT. Similar to RHEB, SGCD might also affect SMC phenotypic switching. It is part of the sarcoglycan complex, linking the SMC plasma membrane to the cytoskeleton. Altered SGCD could affect membrane stability, force transmission, and contractile phenotype [72]. Thus, a mechanical load may produce membrane-cytoskeletal stress that could activate the PI3K-AKT pathway, affecting SMC phenotypic switching. EFEMP2, FBN5 and COL4A1 are extracellular matrix proteins. EFEMP2 (also known as FBN4) is associated with elastic fiber assembly and extracellular matrix organization [73]. FBN5 participates in elastic fiber formation and cell-matrix interactions [73,74]. COL4A1 is a major component of vascular basement membranes, providing structural support for endothelial cells and participating in endothelial–matrix signaling, barrier integrity, and cell adhesion [75]. Alterations in these proteins could modify the aortic wall compliance and the focal adhesion signaling [76], together with a mechanosensitive PI3K-AKT activation. Therefore, it may not merely be an outcome of the pathological process, but it may be part of the initiating feedback loop that activates the PI3K-AKT pathway in response to hemodynamics. We propose that in TBAV animals, the altered hemodynamics induce stress in endothelial cells and SMCs, leading to extracellular matrix remodeling through EFEMP2, FBN5 and COL4A1, modifying the aortic wall mechanics. This would affect the PI3K-AKT pathway, giving rise to SMC phenotype switching and EndMT.

4.2.3. The EndMT Transcription Factor Analysis

Finally, we performed an analysis to find candidate transcription factors that could activate the EndMT program in animals from the T strain. For that, we consulted the Causal Networks analysis from IPA software and the TTRUST database from Enrichr to study candidates jointly (Tables 1 and 2). In the TBAV vs. HTAV comparison, we found nine proteins that could act as transcriptional factors related to EndMT, four of which were present in other comparisons. ZEB was the only transcription factor present in all comparisons, suggesting a genetic and hemodynamic induction, as occurred with CTNNB1. ZEB1 and ZEB2 are transcriptional repressors of endothelial junctions and identity genes, promoting

mesenchymal gene expression [77]. Thus, they are well-established EndMT regulators together with SNAIL/SLUG and TWIST [77]. ZEB may also indicate SMC phenotypic switching. In the presence of ZEB2, resident SMCs turn highly plastic and move from a contractile to a synthetic state, particularly in atherosclerotic coronary arteries [78]. These findings point to a genetic defect in T strain hamsters that may establish a ZEB-permissive cell state affecting CNC-derived SMCs, while disturbed flow in BAV animals increases the magnitude of ZEB activation, inducing EndMT and SMC phenotypic shift. Interestingly, the WNT and PI3K–AKT pathways can converge on ZEB through different routes [79,80].

In the TTAV vs. HTAV comparison, we found four proteins related to SOX genes (SOX1, SOX2, SOX4, and SOX6) that account for genetic factors. SOX4 is particularly interesting because it physically interacts with β-catenin and TCF/LEF proteins to induce EndMT [81,82], which could explain why WNT/β-catenin emerges as the principal genetic pathway in animals from T strain. Furthermore, SOX4 can also regulate CNC cell differentiation, cytoskeletal organization, cell adhesion and extracellular matrix interactions, thereby affecting adult SMC behavior [83]. SOX2 has been shown to promote EndMT, vascular dysfunction, and calcific remodeling [84]. In addition, it may reflect progenitor plasticity and altered CNC state, since it can restrain CNC delamination during development [85]. Thus, SOX2 could identify dedifferentiated or progenitor-like endothelial and SMC states in the aorta of hamsters from T strain that would make cells more responsive to disturbed flow. SOX6 has been recently implicated in vascular SMC phenotypic switching and remodeling [86], so that it could represent a signal for SMC phenotype shift instead of EndMT. SOX1 has been related to neural development [87], but a role in delamination or migration of CNC cells has not been established, so its expression in the ascending aorta cannot be explained. Therefore, we propose that the genetic defect in the T strain alters SOX2/SOX4/SOX6 expression, promoting an arterial wall susceptibility program that specifically affects the SMC phenotype, with SOX2 probably also involved in endothelial plasticity leading to activation of EndMT.

Regarding TBAV vs. TTAV, the comparison that resolves the hemodynamic component, TWIST emerged as a strongly involved transcription factor. TWIST is preferentially induced in regions of low or disturbed shear stress and promotes endothelial inflammation, proliferation, permeability, and EndMT [88]. In vascular endothelial cells, low shear stress can induce TWIST1 through a GATA4-dependent mechanism [88]. Subsequently, TWIST acts with SNAI1/SNAI2 and ZEB1/2 to repress the expression of endothelial genes, activating mesenchymal genes instead [77]. These data support the hypothesis that TWIST is the transcriptional bridge between disturbed flow and EndMT in the TBAV hamster aorta.

5. Limitations

The N1ICD protein expression has been analyzed in control mouse embryos with TAV to validate our previous results with a different species (hamster), which improves the extrapolability of our findings. However, we could not include the N1ICD analysis in hamster embryos with TAV or BAV due to problems with the specificity of N1ICD antibodies. In addition, cell lineage tracing in hamsters is technically unapproachable nowadays. It would be of interest to address the distribution of N1ICD and the expression of JAG1, specifically in CNC cells, in *Notch1* transgenic mice with AP-BAV to confirm its role in this developmental process. Likewise, SHF lineage tracing in *Notch1* transgenic mice would clarify whether CNC-SHF interaction is affected during AP-BAV formation.

The main objective of the reassessment of our previously published proteomic dataset was to assess hints of EndMT in adult hamster aortas from the T strain, but validation of the resulting proteins and signaling pathways was out of scope. It will be of interest to be ap-

proached in future studies, not only to strengthen the developmental program re-expression hypothesis, but to improve its evidence and refine its associated mechanistic model.

Animals from the T strain show a morphological continuum of the aortic valve ranging from TAV to BAV with different degrees of fusion (i.e., intermediate phenotypes) [29,32]. This has also been reported in patients [2]. For this study, we only included pure forms of TAV and BAV, excluding intermediate phenotypes that might modify hemodynamics in different ways since hemodynamic studies are lacking in the hamster model.

6. Conclusions and Hypotheses Generated

1. Murine cardiac OFT septation results from the fusion of the CRs, mediated by a process of EndMT activated by NOTCH in the embryonic endocardium at the center of the CRs.

Hypothesis H1. *The finding of a similar process of OFT septation in hamsters and mice strengthens the hypothesis that EndMT induced by CNC cells is a key developmental process in the formation of TAV and BAV in mammals. The joint analysis of the results from this manuscript and our previous findings provides a robust rationale for an embryonic mechanistic model explaining BAV aortopathy (see below).*

2. The abnormal aorta of hamsters with TAV and AD is characterized by genetic alterations of EndMT-associated proteins and pathways. In addition, animals with BAV exhibit further hemodynamically driven EndMT-specific alterations.

Hypothesis H2. *BAV aortopathy relies on genetic defects that alter the structural stability of the ascending aorta, which is exacerbated by aberrant hemodynamics caused by the anomalous valve morphology.*

3. WNT and PI3K-AKT are the most consistently altered pathways in the aorta of affected hamsters, both associated with genetic and hemodynamic triggers.

Hypothesis H3. *WNT-associated genetic defects predispose the CNC-derived SMCs of the ascending aorta to induce EndMT, while the altered hemodynamic induction of the PI3K-AKT pathway complicates the progression of the aortopathy in BAV individuals.*

4. CTNNB1, KRAS, SLIT3, ZEB, and SOX are the most consistent candidates to be involved in the genetic defect leading to aortic degeneration in the hamster model, while ROCK1, RHEB, EFEMP2, FBN5, COL4A1, SGCD, and TWIST are the most consistent candidates to be hemodynamic triggers.

Hypothesis H4. *The analysis of interactions among these proteins and pathways allows for the development of a mechanistic model for BAV aortopathy initiation (see below) ready to be validated in the hamster model and patients. Testing this hypothesis may lead to the development of new therapeutic strategies and molecular markers of the disease for patient stratification.*

Molecular mechanistic model: In the T strain, a genetic defect alters the CNC-derived SMC differentiation state through a CTNNB1-KRAS-SLIT3-ZEB/SOX-associated program. This predisposes to both BAV formation and structural defects in the wall of the ascending aorta, with Wnt/β-catenin as the principal genetic factor involved. The alteration of blood flow in those animals carrying a BAV activates PI3K-AKT-RHEB/mTOR and RhoA-ROCK1 signaling, with modification of force transmission due to EFEMP2/FBN5/COL4A1 extracellular abnormalities and SGCD-dependent mechanoprotection. These pathways converge

on β-catenin, ZEB, TWIST and other cell plasticity regulators, leading to the activation of parallel, interacting processes of EndMT and SMC phenotypic switching that initiate BAV aortopathy.

Embryonic mechanistic model: during BAV embryonic development, CNC cells invading the pericardial cavity (1) over-induce EndMT during OFT septation, and (2) differentiate into potentially defective aortic CNC-derived SMCs, leading to (1) BAV formation and (2) predisposition to AD. In adults, hemodynamic alterations produced by the anomalous valve prompt an abnormal response of CNC-derived SMCs of the aortic wall. This response recapitulates the CNC-specific developmental program, including EndMT induction and SMC apoptosis in the adult ascending aorta, which leads to AD.

Our hypothesis aligns with the current understanding of the etiology of human BAV aortopathy [1,4,12,14,15,21–23], which is based on the so-called 'fetal gene hypothesis', whereby the embryonic developmental program is reactivated in the adult heart in response to stress [36]. This hypothesis could also apply to BAV-associated valvulopathy, because CNC cells invading the pericardial cavity not only differentiate into aortic SMCs and fibroblasts, but also into a certain proportion of valvular interstitial cells, known to be central in the sclerosis and calcification process involved in aortic valve stenosis [10,89]. Furthermore, EndMT and apoptosis have been identified as key cellular mechanisms in the pathogenesis of BAV-associated stenosis [89].

From a translational standpoint, our novel research findings provide a foundation for mechanism-based interventions targeting the pathways that are active in both embryogenesis and adult remodeling. Consequently, the hamster model could be utilized to assess the therapeutic efficacy of modulating these pathways in decelerating aortic wall degeneration prior to the onset of irreversible dilation. In addition, the present study, in conjunction with our prior investigations, [25–27] offer the potential to identify biomarkers specifically associated with CNC dysfunction, EndMT, SMC phenotype shift, or SMC apoptosis, which may facilitate patient stratification. BAV patients would benefit from earlier and more personalized surveillance of the ascending aorta, even in the absence of AD. This notion is consistent with the hypothesis that some patients carry an intrinsic predisposition to aortopathy, with hemodynamic stress from the dysfunctional valve as a secondary catalyst that accelerates the progression of the disease [4,5]. The identification of biomarkers also proves to be of significant value because the current diagnostic strategies predominantly depend on anatomical and diameter-related assessments, rather than on the intrinsic biological activity of the aortic wall [2].

Supplementary Materials: The following supporting information can be downloaded at: https://www.mdpi.com/article/10.3390/jcdd13110596/s1. Table S1. Specifications of the antibodies used; Table S2. Quantitatively altered proteins in TBAV vs. HTAV groups; Table S3. Altered canonical pathways in TBAV vs. HTAV groups; Table S4. Altered proteins from the TTAV vs. HTAV comparison; Table S5. Significantly altered canonical pathway in TTAV vs. HTAV groups; Table S6. Altered proteins from the TTAV vs. TBAV comparison; Table S7. Significantly altered canonical pathway in TBAV vs. TTAV groups; Table S8. Significantly altered EMT terms detected in Enrichr database from the TTAV vs. TBAV comparison.

Author Contributions: M.T.S.-N.: embryonic experimental data acquisition and analysis, proteomic data reassessment, writing, review, and editing. B.P.-V.: proteomic data reassessment, writing, review, and editing. A.C.D.: review and editing. B.F.: conceptualization, funding acquisition, supervision, writing, review and editing. All authors have read and agreed to the published version of the manuscript.

Funding: This work was supported by the University of Malaga (PPRO-BIO203-G-2023 (BIO203-G-FEDER)), Junta de Andalucía Consejería de Universidad, Investigación e Innovación (BIO203) and Ministerio de Ciencia e Innovación (JDC2023-051982-I to M.T.S.-N).

Institutional Review Board Statement: Animals were handled in accordance with the European guidelines (Directive 2010/63/EU) and Spanish regulations (R.D. 53/2013; B.O.E. 01.02.2013) for the protection of experimental animals. The experimental protocols were approved by the Ethics Committee of Animal Experiments of the University of Málaga (CEUMA; Ethics authorization number: 25/08/2021/118, approved on 8 September 2021) and CNIC Animal Experimentation Ethics Committee (PROEX 054.6/25, approved on 25 March 2025). All methods are reported in accordance with ARRIVE guidelines (https://arriveguidelines.org (accessed on 27 October 2026)).

Informed Consent Statement: Not applicable.

Data Availability Statement: The proteomic dataset is available in the PRIDE database (Proteomics Identifications Database) with reference: 1-20241211-200357-3535972.

Conflicts of Interest: The authors declare no conflicts of interest.

References

1. Thiene, G.; Fraccaro, C.; Tarantini, G.; Basso, C. *Bicuspid Aortic Valve Syndrome: A Not so Benign Congenital Heart Disease*; Springer Nature: Cham, Switzerland, 2025; ISBN 978-3-031-85589-4.
2. Michelena, H.I.; Della Corte, A.; Evangelista, A.; Maleszewski, J.J.; Edwards, W.D.; Roman, M.J.; Devereux, R.B.; Fernández, B.; Asch, F.M.; Barker, A.J.; et al. International Consensus Statement on Nomenclature and Classification of the Congenital Bicuspid Aortic Valve and Its Aortopathy, for Clinical, Surgical, Interventional and Research Purposes. *Eur. J. Cardio-Thorac. Surg.* **2021**, *60*, 448–476. [CrossRef] [PubMed]
3. Grewal, N.; Klautz, R.J.M.; Poelmann, R.E. Intrinsic Histological and Morphological Abnormalities of the Pediatric Thoracic Aorta in Bicuspid Aortic Valve Patients Are Predictive for Future Aortopathy. *Pathol. Res. Pract.* **2023**, *248*, 154620. [CrossRef] [PubMed]
4. Prakash, S.K.; Bossé, Y.; Muehlschlegel, J.D.; Michelena, H.I.; Limongelli, G.; Della Corte, A.; Pluchinotta, F.R.; Russo, M.G.; Evangelista, A.; Benson, D.W.; et al. A Roadmap to Investigate the Genetic Basis of Bicuspid Aortic Valve and Its Complications: Insights from the International BAVCon (Bicuspid Aortic Valve Consortium). *J. Am. Coll. Cardiol.* **2014**, *64*, 832–839. [CrossRef] [PubMed]
5. Michelena, H.I.; Della Corte, A.; Evangelista, A.; Maleszewski, J.J.; Enriquez-Sarano, M.; Bax, J.J.; Otto, C.M.; Schäfers, H.-J. Speaking a Common Language: Introduction to a Standard Terminology for the Bicuspid Aortic Valve and Its Aortopathy. *Prog. Cardiovasc. Dis.* **2020**, *63*, 419–424. [CrossRef] [PubMed]
6. Padang, R.; Bannon, P.G.; Jeremy, R.; Richmond, D.R.; Semsarian, C.; Vallely, M.; Wilson, M.; Yan, T.D. The Genetic and Molecular Basis of Bicuspid Aortic Valve Associated Thoracic Aortopathy: A Link to Phenotype Heterogeneity. *Ann. Cardiothorac. Surg.* **2013**, *2*, 83–91. [CrossRef] [PubMed]
7. Sophocleous, F.; Milano, E.G.; Pontecorboli, G.; Chivasso, P.; Caputo, M.; Rajakaruna, C.; Bucciarelli-Ducci, C.; Emanueli, C.; Biglino, G. Enlightening the Association between Bicuspid Aortic Valve and Aortopathy. *J. Cardiovasc. Dev. Dis.* **2018**, *5*, 21. [CrossRef] [PubMed]
8. Hinton, R.B. Bicuspid Aortic Valve and Thoracic Aortic Aneurysm: Three Patient Populations, Two Disease Phenotypes, and One Shared Genotype. *Cardiol. Res. Pract.* **2012**, *2012*, 926975. [CrossRef] [PubMed]
9. Kirby, M.L.; Gale, T.F.; Stewart, D.E. Neural Crest Cells Contribute to Normal Aorticopulmonary Septation. *Science* **1983**, *220*, 1059–1061. [CrossRef] [PubMed]
10. Eley, L.; Alqahtani, A.M.; MacGrogan, D.; Richardson, R.V.; Murphy, L.; Salguero-Jimenez, A.; Sintes Rodriguez San Pedro, M.; Tiurma, S.; McCutcheon, L.; Gilmore, A.; et al. A Novel Source of Arterial Valve Cells Linked to Bicuspid Aortic Valve without Raphe in Mice. *eLife* **2018**, *7*, e34110. [CrossRef] [PubMed]
11. Sawada, H.; Rateri, D.L.; Moorleghen, J.J.; Majesky, M.W.; Daugherty, A. Smooth Muscle Cells Derived from Second Heart Field and Cardiac Neural Crest Reside in Spatially Distinct Domains in the Media of the Ascending Aorta-Brief Report. *Arterioscler. Thromb. Vasc. Biol.* **2017**, *37*, 1722–1726. [CrossRef] [PubMed]
12. Jiao, J.; Xiong, W.; Wang, L.; Yang, J.; Qiu, P.; Hirai, H.; Shao, L.; Milewicz, D.; Chen, Y.E.; Yang, B. Differentiation Defect in Neural Crest-Derived Smooth Muscle Cells in Patients with Aortopathy Associated with Bicuspid Aortic Valves. *EBioMedicine* **2016**, *10*, 282–290. [CrossRef] [PubMed]
13. Nistri, S.; Giusti, B.; Pepe, G.; Cademartiri, F. Another Piece in the Puzzle of Bicuspid Aortic Valve Syndrome. *Eur. Heart J. Cardiovasc. Imaging* **2016**, *17*, 1248–1249. [CrossRef] [PubMed]
14. Maleki, S.; Poujade, F.-A.; Bergman, O.; Gådin, J.R.; Simon, N.; Lång, K.; Franco-Cereceda, A.; Body, S.C.; Björck, H.M.; Eriksson, P. Endothelial/Epithelial Mesenchymal Transition in Ascending Aortas of Patients with Bicuspid Aortic Valve. *Front. Cardiovasc. Med.* **2019**, *6*, 182. [CrossRef] [PubMed]

15. Björck, H.M.; Du, L.; Pulignani, S.; Paloschi, V.; Lundströmer, K.; Kostina, A.S.; Österholm, C.; Malashicheva, A.; Kostareva, A.; Evangelista, A.; et al. Altered DNA Methylation Indicates an Oscillatory Flow Mediated Epithelial-to-Mesenchymal Transition Signature in Ascending Aorta of Patients with Bicuspid Aortic Valve. *Sci. Rep.* **2018**, *8*, 2777. [CrossRef] [PubMed]
16. Yang, J.; Antin, P.; Berx, G.; Blanpain, C.; Brabletz, T.; Bronner, M.; Campbell, K.; Cano, A.; Casanova, J.; Christofori, G.; et al. Guidelines and Definitions for Research on Epithelial-Mesenchymal Transition. *Nat. Rev. Mol. Cell Biol.* **2020**, *21*, 341–352. [CrossRef] [PubMed]
17. Zhang, Z.; Fang, Z.; Ge, J.; Li, H. Endothelial-to-Mesenchymal Transition in Cardiovascular Diseases. *Trends Mol. Med.* **2025**, *31*, 992–1007. [CrossRef] [PubMed]
18. Hall, I.F.; Aikawa, E.; Sluimer, J.; Baker, A.H.; Kovacic, J.C. Endothelial to Mesenchymal Transition in Cardiovascular Diseases: Molecular Insights and Clinical Perspectives. *Eur. Heart J.* **2026**, *47*, 1144–1158. [CrossRef] [PubMed]
19. Gehlen, J.; Stundl, A.; Debiec, R.; Fontana, F.; Krane, M.; Sharipova, D.; Nelson, C.P.; Al-Kassou, B.; Giel, A.-S.; Sinning, J.-M.; et al. Elucidation of the Genetic Causes of Bicuspid Aortic Valve Disease. *Cardiovasc. Res.* **2023**, *119*, 857–866. [CrossRef] [PubMed]
20. Kostina, A.S.; Uspensky, V.E.; Irtyuga, O.B.; Ignatieva, E.V.; Freylikhman, O.; Gavriliuk, N.D.; Moiseeva, O.M.; Zhuk, S.; Tomilin, A.; Kostareva, A.A.; et al. Notch-Dependent EMT Is Attenuated in Patients with Aortic Aneurysm and Bicuspid Aortic Valve. *Biochim. Biophys. Acta* **2016**, *1862*, 733–740. [CrossRef] [PubMed]
21. Freiholtz, D.; Bergman, O.; Lång, K.; Poujade, F.-A.; Paloschi, V.; Granath, C.; Lindeman, J.H.N.; Olsson, C.; Franco-Cereceda, A.; Eriksson, P.; et al. Bicuspid Aortic Valve Aortopathy Is Characterized by Embryonic Epithelial to Mesenchymal Transition and Endothelial Instability. *J. Mol. Med.* **2023**, *101*, 801–811. [CrossRef] [PubMed]
22. Maleki, S.; Kjellqvist, S.; Paloschi, V.; Magné, J.; Branca, R.M.M.; Du, L.; Hultenby, K.; Petrini, J.; Fuxe, J.; MIBAVA Leducq Consortium; et al. Mesenchymal State of Intimal Cells May Explain Higher Propensity to Ascending Aortic Aneurysm in Bicuspid Aortic Valves. *Sci. Rep.* **2016**, *6*, 35712. [CrossRef] [PubMed]
23. Kjellqvist, S.; Maleki, S.; Olsson, T.; Chwastyniak, M.; Branca, R.M.M.; Lehtiö, J.; Pinet, F.; Franco-Cereceda, A.; Eriksson, P. A Combined Proteomic and Transcriptomic Approach Shows Diverging Molecular Mechanisms in Thoracic Aortic Aneurysm Development in Patients with Tricuspid- and Bicuspid Aortic Valve. *Mol. Cell. Proteom. MCP* **2013**, *12*, 407–425. [CrossRef] [PubMed]
24. Fernández, B.; Durán, A.C.; Fernández-Gallego, T.; Fernández, M.C.; Such, M.; Arqué, J.M.; Sans-Coma, V. Bicuspid Aortic Valves with Different Spatial Orientations of the Leaflets Are Distinct Etiological Entities. *J. Am. Coll. Cardiol.* **2009**, *54*, 2312–2318. [CrossRef] [PubMed]
25. Soto-Navarrete, M.T.; Pozo-Vilumbrales, B.; López-Unzu, M.Á.; Martín-Chaves, L.; Durán, A.C.; Fernández, B. Endocardial-to-Mesenchymal Transition Underlies Cardiac Outflow Tract Septation and Bicuspid Aortic Valve Formation in the Syrian Hamster Model. *Sci. Rep.* **2025**, *15*, 8583. [CrossRef] [PubMed]
26. Soto-Navarrete, M.T.; Pozo-Vilumbrales, B.; López-Unzu, M.Á.; Rueda-Martínez, C.; Fernández, M.C.; Durán, A.C.; Pavón-Morón, F.J.; Rodríguez-Capitán, J.; Fernández, B. Experimental Evidence of the Genetic Hypothesis on the Etiology of Bicuspid Aortic Valve Aortopathy in the Hamster Model. *Front. Cardiovasc. Med.* **2022**, *9*, 928362. [CrossRef] [PubMed]
27. Pozo-Vilumbrales, B.; Martín-Chaves, L.; López-Unzu, M.A.; Soto-Navarrete, M.T.; Pavón-Morón, F.J.; Rodríguez-Capitán, J.; Fernández, B. Unraveling the Molecular Complexity of Bicuspid Aortopathy: Lessons from Comparative Proteomics. *Biochim. Biophys. Acta Mol. Basis Dis.* **2025**, *1871*, 167679. [CrossRef] [PubMed]
28. Sans-Coma, V.; Cardo, M.; Durán, A.C.; Franco, D.; Fernández, B.; Arqué, J.M. Evidence for a Quantitative Genetic Influence on the Formation of Aortic Valves with Two Leaflets in the Syrian Hamster. *Cardiol. Young* **1993**, *3*, 132–140. [CrossRef]
29. Sans-Coma, V.; Fernández, B.; Durán, A.C.; Thiene, G.; Arqué, J.M.; Muñoz-Chápuli, R.; Cardo, M. Fusion of Valve Cushions as a Key Factor in the Formation of Congenital Bicuspid Aortic Valves in Syrian Hamsters. *Anat. Rec.* **1996**, *244*, 490–498. [CrossRef]
30. Sans-Coma, V.; Carmen Fernández, M.; Fernández, B.; Durán, A.C.; Anderson, R.H.; Arqué, J.M. Genetically Alike Syrian Hamsters Display Both Bifoliate and Trifoliate Aortic Valves. *J. Anat.* **2012**, *220*, 92–101. [CrossRef] [PubMed]
31. Soto-Navarrete, M.T.; López-Unzu, M.Á.; Durán, A.C.; Fernández, B. Embryonic Development of Bicuspid Aortic Valves. *Prog. Cardiovasc. Dis.* **2020**, *63*, 407–418. [CrossRef] [PubMed]
32. Fernández, B.; Soto-Navarrete, M.T.; López-García, A.; López-Unzu, M.Á.; Durán, A.C.; Fernández, M.C. Bicuspid Aortic Valve in 2 Model Species and Review of the Literature. *Vet. Pathol.* **2020**, *57*, 321–331. [CrossRef] [PubMed]
33. Młynarczyk, M.; Kasacka, I. The Role of the Wnt/β-Catenin Pathway and the Functioning of the Heart in Arterial Hypertension—A Review. *Adv. Med. Sci.* **2022**, *67*, 87–94. [CrossRef] [PubMed]
34. Timmerman, L.A.; Grego-Bessa, J.; Raya, A.; Bertrán, E.; Pérez-Pomares, J.M.; Díez, J.; Aranda, S.; Palomo, S.; McCormick, F.; Izpisúa-Belmonte, J.C.; et al. Notch Promotes Epithelial-Mesenchymal Transition during Cardiac Development and Oncogenic Transformation. *Genes Dev.* **2004**, *18*, 99–115. [CrossRef] [PubMed]
35. MacGrogan, D.; D'Amato, G.; Travisano, S.; Martinez-Poveda, B.; Luxán, G.; Del Monte-Nieto, G.; Papoutsi, T.; Sbroggio, M.; Bou, V.; Gomez-Del Arco, P.; et al. Sequential Ligand-Dependent Notch Signaling Activation Regulates Valve Primordium Formation and Morphogenesis. *Circ. Res.* **2016**, *118*, 1480–1497. [CrossRef] [PubMed]

36. Porrello, E.R.; Lee, C.J.M.; Foo, R.S.Y.; Elliott, D.A. Transcriptional Regulation in Heart Development, Disease and Regeneration: Reassessing the Fetal Gene Hypothesis. *Nat. Rev. Cardiol.* **2026**, *23*, 183–196. [CrossRef] [PubMed]
37. Wang, J.; Zhang, W.; Jiang, S.; Wang, Z.; Li, Y.; Li, T. The Regulation of Endothelial-to-Mesenchymal Transition in Endocardial Cushion Development: Signaling Pathways and Transcription Factors. *Differ. Res. Biol. Divers.* **2026**, *151*, 100987. [CrossRef] [PubMed]
38. Schussler, O.; Gharibeh, L.; Mootoosamy, P.; Murith, N.; Tien, V.; Rougemont, A.-L.; Sologashvili, T.; Suuronen, E.; Lecarpentier, Y.; Ruel, M. Cardiac Neural Crest Cells: Their Rhombomeric Specification, Migration, and Association with Heart and Great Vessel Anomalies. *Cell. Mol. Neurobiol.* **2021**, *41*, 403–429. [CrossRef] [PubMed]
39. Buckingham, M.; Meilhac, S.; Zaffran, S. Building the Mammalian Heart from Two Sources of Myocardial Cells. *Nat. Rev. Genet.* **2005**, *6*, 826–835. [CrossRef] [PubMed]
40. Kelly, R.G.; Buckingham, M.E.; Moorman, A.F. Heart Fields and Cardiac Morphogenesis. *Cold Spring Harb. Perspect. Med.* **2014**, *4*, a015750. [CrossRef] [PubMed]
41. Phillips, H.M.; Mahendran, P.; Singh, E.; Anderson, R.H.; Chaudhry, B.; Henderson, D.J. Neural Crest Cells Are Required for Correct Positioning of the Developing Outflow Cushions and Pattern the Arterial Valve Leaflets. *Cardiovasc. Res.* **2013**, *99*, 452–460. [CrossRef] [PubMed]
42. Anderson, R.H.; Chaudhry, B.; Mohun, T.J.; Bamforth, S.D.; Hoyland, D.; Phillips, H.M.; Webb, S.; Moorman, A.F.M.; Brown, N.A.; Henderson, D.J. Normal and Abnormal Development of the Intrapericardial Arterial Trunks in Humans and Mice. *Cardiovasc. Res.* **2012**, *95*, 108–115. [CrossRef] [PubMed]
43. Poelmann, R.E.; Mikawa, T.; Gittenberger-de Groot, A.C. Neural Crest Cells in Outflow Tract Septation of the Embryonic Chicken Heart: Differentiation and Apoptosis. *Dev. Dyn. Off. Publ. Am. Assoc. Anat.* **1998**, *212*, 373–384. [CrossRef]
44. Sharma, P.R.; Anderson, R.H.; Copp, A.J.; Henderson, D.J. Spatiotemporal Analysis of Programmed Cell Death during Mouse Cardiac Septation. *Anat. Rec. A Discov. Mol. Cell. Evol. Biol.* **2004**, *277*, 355–369. [CrossRef] [PubMed]
45. Plein, A.; Calmont, A.; Fantin, A.; Denti, L.; Anderson, N.A.; Scambler, P.J.; Ruhrberg, C. Neural Crest–Derived SEMA3C Activates Endothelial NRP1 for Cardiac Outflow Tract Septation. *J. Clin. Investig.* **2015**, *125*, 2661–2676. [CrossRef] [PubMed]
46. Anderson, R.H.; Lamers, W.H.; Hikspoors, J.P.J.M.; Mohun, T.J.; Bamforth, S.D.; Chaudhry, B.; Eley, L.; Kerwin, J.; Crosier, M.; Henderson, D.J. Development of the Arterial Roots and Ventricular Outflow Tracts. *J. Anat.* **2024**, *244*, 497–513. [CrossRef] [PubMed]
47. Kopan, R.; Ilagan, M.X.G. The Canonical Notch Signaling Pathway: Unfolding the Activation Mechanism. *Cell* **2009**, *137*, 216–233. [CrossRef] [PubMed]
48. Jain, R.; Engleka, K.A.; Rentschler, S.L.; Manderfield, L.J.; Li, L.; Yuan, L.; Epstein, J.A. Cardiac Neural Crest Orchestrates Remodeling and Functional Maturation of Mouse Semilunar Valves. *J. Clin. Investig.* **2011**, *121*, 422–430. [CrossRef] [PubMed]
49. High, F.A.; Zhang, M.; Proweller, A.; Tu, L.; Parmacek, M.S.; Pear, W.S.; Epstein, J.A. An Essential Role for Notch in Neural Crest during Cardiovascular Development and Smooth Muscle Differentiation. *J. Clin. Investig.* **2007**, *117*, 353–363. [CrossRef] [PubMed]
50. Martínez-Vargas, J.; Ventura, J.; Machuca, Á.; Muñoz-Muñoz, F.; Fernández, M.C.; Soto-Navarrete, M.T.; Durán, A.C.; Fernández, B. Cardiac, Mandibular and Thymic Phenotypical Association Indicates That Cranial Neural Crest Underlies Bicuspid Aortic Valve Formation in Hamsters. *PLoS ONE* **2017**, *12*, e0183556. [CrossRef] [PubMed]
51. Garg, V.; Muth, A.N.; Ransom, J.F.; Schluterman, M.K.; Barnes, R.; King, I.N.; Grossfeld, P.D.; Srivastava, D. Mutations in NOTCH1 Cause Aortic Valve Disease. *Nature* **2005**, *437*, 270–274. [CrossRef] [PubMed]
52. Fedak, P.W.M.; Verma, S.; David, T.E.; Leask, R.L.; Weisel, R.D.; Butany, J. Clinical and Pathophysiological Implications of a Bicuspid Aortic Valve. *Circulation* **2002**, *106*, 900–904. [CrossRef] [PubMed]
53. Cripe, L.; Andelfinger, G.; Martin, L.J.; Shooner, K.; Benson, D.W. Bicuspid Aortic Valve Is Heritable. *J. Am. Coll. Cardiol.* **2004**, *44*, 138–143. [CrossRef] [PubMed]
54. Raj, A.; Rifkin, S.A.; Andersen, E.; Van Oudenaarden, A. Variability in Gene Expression Underlies Incomplete Penetrance. *Nature* **2010**, *463*, 913–918. [CrossRef] [PubMed]
55. Liebner, S.; Cattelino, A.; Gallini, R.; Rudini, N.; Iurlaro, M.; Piccolo, S.; Dejana, E. β-Catenin Is Required for Endothelial-Mesenchymal Transformation during Heart Cushion Development in the Mouse. *J. Cell Biol.* **2004**, *166*, 359–367. [CrossRef] [PubMed]
56. Puertas-Umbert, L.; Varona, S.; Ballester-Servera, C.; Alonso, J.; Aguiló, S.; Orriols, M.; Martínez-Martínez, E.; Rodríguez-Sinovas, A.; Martínez-González, J.; Rodríguez, C. Activation of Wnt/β-Catenin Signaling in Abdominal Aortic Aneurysm: A Potential Therapeutic Opportunity? *Genes Dis.* **2023**, *10*, 639–642. [CrossRef] [PubMed]
57. Li, C.; Wang, K.; Fang, J.; Qin, L.; Ling, Q.; Yu, Y. TRIM25 Activates Wnt/β-Catenin Signalling by Destabilising MAT2A mRNA to Drive Thoracic Aortic Aneurysm Development. *Hum. Mol. Genet.* **2024**, *33*, 1890–1899. [CrossRef] [PubMed]
58. Larue, L.; Bellacosa, A. Epithelial-Mesenchymal Transition in Development and Cancer: Role of Phosphatidylinositol 3′ Kinase/AKT Pathways. *Oncogene* **2005**, *24*, 7443–7454. [CrossRef] [PubMed]

59. Kim, R.; Chang, W. Endothelial-to-Mesenchymal Transition in Health and Disease: Molecular Insights and Therapeutic Implications. *Int. J. Mol. Sci.* **2025**, *26*, 11724. [CrossRef] [PubMed]
60. Beamish, J.A.; He, P.; Kottke-Marchant, K.; Marchant, R.E. Molecular Regulation of Contractile Smooth Muscle Cell Phenotype: Implications for Vascular Tissue Engineering. *Tissue Eng. Part B Rev.* **2010**, *16*, 467–491. [CrossRef] [PubMed]
61. Dong, C.X.; Malecki, C.; Robertson, E.; Hambly, B.; Jeremy, R. Molecular Mechanisms in Genetic Aortopathy-Signaling Pathways and Potential Interventions. *Int. J. Mol. Sci.* **2023**, *24*, 1795. [CrossRef] [PubMed]
62. Fang, D.; Hawke, D.; Zheng, Y.; Xia, Y.; Meisenhelder, J.; Nika, H.; Mills, G.B.; Kobayashi, R.; Hunter, T.; Lu, Z. Phosphorylation of Beta-Catenin by AKT Promotes Beta-Catenin Transcriptional Activity. *J. Biol. Chem.* **2007**, *282*, 11221–11229. [CrossRef] [PubMed]
63. Gao, Z.; Kim, G.H.; Mackinnon, A.C.; Flagg, A.E.; Bassett, B.; Earley, J.U.; Svensson, E.C. Ets1 Is Required for Proper Migration and Differentiation of the Cardiac Neural Crest. *Development* **2010**, *137*, 1543–1551. [CrossRef] [PubMed]
64. Prasad, M.S.; Charney, R.M.; García-Castro, M.I. Specification and Formation of the Neural Crest: Perspectives on Lineage Segregation. *Genesis* **2019**, *57*, e23276. [CrossRef] [PubMed]
65. Wang, G.; Li, Y.; Wang, X.; Han, Z.; Chuai, M.; Wang, L.; Ho Lee, K.K.; Geng, J.; Yang, X. Slit/Robo1 Signaling Regulates Neural Tube Development by Balancing Neuroepithelial Cell Proliferation and Differentiation. *Exp. Cell Res.* **2013**, *319*, 1083–1093. [CrossRef] [PubMed]
66. Li, Y.; Zhang, X.; Wang, X.; Wang, G.; Chuai, M.; Münsterberg, A.; Yang, X. Robo Signaling Regulates the Production of Cranial Neural Crest Cells. *Exp. Cell Res.* **2017**, *361*, 73–84. [CrossRef] [PubMed]
67. De Calisto, J.; Araya, C.; Marchant, L.; Riaz, C.F.; Mayor, R. Essential Role of Non-Canonical Wnt Signalling in Neural Crest Migration. *Development* **2005**, *132*, 2587–2597. [CrossRef] [PubMed]
68. Horitani, K.; Shiojima, I. Wnt Signaling in Cardiac Development and Heart Diseases. *In Vitro Cell. Dev. Biol. Anim.* **2024**, *60*, 482–488. [CrossRef] [PubMed]
69. Soriano, O.; Alcón-Pérez, M.; Vicente-Manzanares, M.; Castellano, E. The Crossroads between RAS and RHO Signaling Pathways in Cellular Transformation, Motility and Contraction. *Genes* **2021**, *12*, 819. [CrossRef] [PubMed]
70. Elmarasi, M.; Elmakaty, I.; Elsayed, B.; Elsayed, A.; Zein, J.A.; Boudaka, A.; Eid, A.H. Phenotypic Switching of Vascular Smooth Muscle Cells in Atherosclerosis, Hypertension, and Aortic Dissection. *J. Cell. Physiol.* **2024**, *239*, e31200. [CrossRef] [PubMed]
71. Dibble, C.C.; Cantley, L.C. Regulation of mTORC1 by PI3K Signaling. *Trends Cell Biol.* **2015**, *25*, 545–555. [CrossRef] [PubMed]
72. Kalayinia, S.; Poopak, A.; Soveizi, M.; Maleki, M. From Gene to Heart: The Impact of a Novel SGCD Variant in Familial Dilated Cardiomyopathy. *BMC Med. Genom.* **2026**, *19*, 67. [CrossRef] [PubMed]
73. Shin, S.J.; Yanagisawa, H. Recent Updates on the Molecular Network of Elastic Fiber Formation. *Essays Biochem.* **2019**, *63*, 365–376. [CrossRef] [PubMed]
74. Yanagisawa, H.; Schluterman, M.K.; Brekken, R.A. Fibulin-5, an Integrin-Binding Matricellular Protein: Its Function in Development and Disease. *J. Cell Commun. Signal.* **2009**, *3*, 337–347. [CrossRef] [PubMed]
75. Volonghi, I.; Pezzini, A.; Del Zotto, E.; Giossi, A.; Costa, P.; Ferrari, D.; Padovani, A. Role of COL4A1 in Basement-Membrane Integrity and Cerebral Small-Vessel Disease. The COL4A1 Stroke Syndrome. *Curr. Med. Chem.* **2010**, *17*, 1317–1324. [CrossRef] [PubMed]
76. Steffensen, L.B.; Stubbe, J.; Lindholt, J.S.; Beck, H.C.; Overgaard, M.; Bloksgaard, M.; Genovese, F.; Holm Nielsen, S.; Tha, M.L.T.; Bang-Moeller, S.K.; et al. Basement Membrane Collagen IV Deficiency Promotes Abdominal Aortic Aneurysm Formation. *Sci. Rep.* **2021**, *11*, 12903. [CrossRef] [PubMed]
77. Welch-Reardon, K.M.; Wu, N.; Hughes, C.C.W. A Role for Partial Endothelial-Mesenchymal Transitions in Angiogenesis? *Arterioscler. Thromb. Vasc. Biol.* **2015**, *35*, 303–308. [CrossRef] [PubMed]
78. Cheng, P.; Wirka, R.C.; Shoa Clarke, L.; Zhao, Q.; Kundu, R.; Nguyen, T.; Nair, S.; Sharma, D.; Kim, H.-J.; Shi, H.; et al. ZEB2 Shapes the Epigenetic Landscape of Atherosclerosis. *Circulation* **2022**, *145*, 469–485. [CrossRef] [PubMed]
79. Sánchez-Tilló, E.; De Barrios, O.; Siles, L.; Cuatrecasas, M.; Castells, A.; Postigo, A. β-Catenin/TCF4 Complex Induces the Epithelial-to-Mesenchymal Transition (EMT)-Activator ZEB1 to Regulate Tumor Invasiveness. *Proc. Natl. Acad. Sci. USA* **2011**, *108*, 19204–19209. [CrossRef] [PubMed]
80. Moghbeli, M. PI3K/AKT Pathway as a Pivotal Regulator of Epithelial-Mesenchymal Transition in Lung Tumor Cells. *Cancer Cell Int.* **2024**, *24*, 165. [CrossRef] [PubMed]
81. Sinner, D.; Kordich, J.J.; Spence, J.R.; Opoka, R.; Rankin, S.; Lin, S.-C.J.; Jonatan, D.; Zorn, A.M.; Wells, J.M. Sox17 and Sox4 Differentially Regulate Beta-Catenin/T-Cell Factor Activity and Proliferation of Colon Carcinoma Cells. *Mol. Cell. Biol.* **2007**, *27*, 7802–7815. [CrossRef] [PubMed]
82. Cheng, C.K.; Lin, X.; Pu, Y.; Tse, J.K.Y.; Wang, Y.; Zhang, C.-L.; Cao, X.; Lau, C.W.; Huang, J.; He, L.; et al. SOX4 Is a Novel Phenotypic Regulator of Endothelial Cells in Atherosclerosis Revealed by Single-Cell Analysis. *J. Adv. Res.* **2023**, *43*, 187–203. [CrossRef] [PubMed]
83. Paul, M.H.; Harvey, R.P.; Wegner, M.; Sock, E. Cardiac Outflow Tract Development Relies on the Complex Function of Sox4 and Sox11 in Multiple Cell Types. *Cell. Mol. Life Sci. CMLS* **2014**, *71*, 2931–2945. [CrossRef] [PubMed]

84. Guihard, P.J.; Yao, J.; Blazquez-Medela, A.M.; Iruela-Arispe, L.; Boström, K.I.; Yao, Y. Endothelial-Mesenchymal Transition in Vascular Calcification of Ins2Akita/+ Mice. *PLoS ONE* **2016**, *11*, e0167936. [CrossRef] [PubMed]
85. Mandalos, N.; Rhinn, M.; Granchi, Z.; Karampelas, I.; Mitsiadis, T.; Economides, A.N.; Dollé, P.; Remboutsika, E. Sox2 Acts as a Rheostat of Epithelial to Mesenchymal Transition during Neural Crest Development. *Front. Physiol.* **2014**, *5*, 345. [CrossRef] [PubMed]
86. Ling, Q.; Dong, X.; Mao, L.; Huang, C.; Cong, L.; Zhang, H.; Cai, J.; Chen, Z. SOX6 Enhances Vascular Smooth Muscle Cell Phenotypic Switching and Elevates Blood Pressure by Activating Autophagy. *Anim. Model. Exp. Med.* **2025**, *8*, 1400–1415. [CrossRef] [PubMed]
87. Venere, M.; Han, Y.-G.; Bell, R.; Song, J.S.; Alvarez-Buylla, A.; Blelloch, R. Sox1 Marks an Activated Neural Stem/Progenitor Cell in the Hippocampus. *Development* **2012**, *139*, 3938–3949. [CrossRef] [PubMed]
88. Mahmoud, M.M.; Kim, H.R.; Xing, R.; Hsiao, S.; Mammoto, A.; Chen, J.; Serbanovic-Canic, J.; Feng, S.; Bowden, N.P.; Maguire, R.; et al. TWIST1 Integrates Endothelial Responses to Flow in Vascular Dysfunction and Atherosclerosis. *Circ. Res.* **2016**, *119*, 450–462. [CrossRef] [PubMed]
89. Dutta, P.; Lincoln, J. Calcific Aortic Valve Disease: A Developmental Biology Perspective. *Curr. Cardiol. Rep.* **2018**, *20*, 21. [CrossRef] [PubMed]

Disclaimer/Publisher's Note: The statements, opinions and data contained in all publications are solely those of the individual author(s) and contributor(s) and not of MDPI and/or the editor(s). MDPI and/or the editor(s) disclaim responsibility for any injury to people or property resulting from any ideas, methods, instructions or products referred to in the content.